Tech Science Press

Fabrication and Application of CeO_2 Nanostructure with Different Morphologies: A Review

Xiaofei Cao[1], Shuo Zhao[1], ShuJun Yan[2], Jun Hu[1,*] and Yong Dan[1,*]

[1]School of Chemical Engineering, Northwest University, Xi'an, 710069, China
[2]National Energy Group Ningxia Coal Industry Co., Ltd., Yinchuan, 750001, China
*Corresponding Authors: Jun Hu. Email: hujun32456@163.com; Yong Dan. Email: danyong11@163.com

Abstract: CeO_2, as a significant functional material, Has a widespread application in many fields due to its excellent properties. In this review, we sum up a serious of methods to prepare and differentiate nanostructured cerium oxide with various morphologies based on dimensionality and its main applications in industry. We mainly summary the different strategies to synthetic the CeO_2 with 0-D, 1-D, 2-D and 3-D and the key parameters which may affect the nanostructures. We hope that this review helps researchers master can look up CeO_2 related knowledge more quickly upon the synthetic methods and comparing various morphologies or fabricating ways to explore more convenient and economical procedures when they embark on new research on synthesis cerium oxide.

Keywords: Cerium oxide; synthesis; morphology; application

1 Introduction

As an important functional material, CeO_2 has been widely investigated due to its excellent properties. In the cell, Ce^{4+} is arranged in a face-centred cubic lattice, and O^{2-} occupies all tetrahedral positions, so there are 8 O^{2-} around each Ce^{4+}, and each O^{2-} coordinates with 4 Ce^{4+}. Because there are many cubic voids in the structure, it can be called an open structure. The open structure is characterized by fast ionic conductors, which allow ions to spread rapidly. After reduction at high temperature (T > 950°C), CeO_2 was transformed into CeO_2-x oxide with oxygen vacancy and non-stoichiometric ratio (0 < x < 0.5), while at low temperature (T < 450°C) CeO_2 could form a series of compounds with different compositions. It is worth noting that even lose lots of oxygen from the lattice, the formation of much oxygen vacancy, CeO_2-x can still keep the fluorite crystal structure, this kind of metastable oxides when exposed to the oxidation environment and susceptible to oxidation of CeO_2. Therefore, CeO_2 has superior storage and release oxygen function and redox reaction ability, CeO_2 also has good chemical stability and high-temperature oxygen vacancy diffusion ability, 970°C for oxygen vacancy diffusion coefficient of 10 to 5 cm^2/s [1]. CeO_2, as a significant rare earth oxide functional material, has been widely used in many fields. Especially, nano cerium oxide has attracted for decades due to its novel physical and chemical properties. Both the super-redox property and oxygen storage-release capacity make it, to a large extent, suitable for wide applications. For instance, it is widely used in solar cells [2,3], three-way catalysts (TWCs) [4,5], ultraviolet absorbers [6], solid oxide fuel cell electrolyte materials [7,8], optical coatings

[9], glass polishing agents [10], magnetic materials [11], superhydrophobic coatings and so on. Among these applications, the catalytic application is of vital significance to industrial production. Recently, morphology engineering of catalyst nanoparticles appeared to be a successful strategy to tailor catalytic performance without affecting catalyst composition. Accordingly, it is of vital importance to fabricate various morphologies of CeO_2 nanostructures. However, in recent materials research, it is still a great challenge to fabricate nanocrystalline with desired dimensions and morphology for different application. Particularly, the synthesis of 2-D CeO_2 nanostructure is more difficult than 1-D nanostructure, which mainly due to that when the crystal growth in 2-D dimensions, it is difficult to realize directional control, especially in solution-phase. And the reason why synthesis of nanosheet or nanoplates in the liquid-phase is difficult is that the CeO_2 lacks of intrinsic driving force in 2-D growth for its cubic crystal structure [12]. As well, it is still a challenge to realize controlled organization from nanoscales units [13–15], some strategies should be taken to assemble into ordered 3-D nanostructures in order to develop a nanodevice with high performance. Hitherto, a variety of micro/nanostructure CeO_2 with different morphologies have been successfully fabricated such as nanoparticles, nanosphere, nanowires, nanorods, nanotube, nanoplates, nanosheets, nanocubes, nano hexagonal prisms, nano-octahedrons, flower-like nanorod, etc. In this review, we mainly summarise different strategies to synthetic the nanostructure CeO_2 and explore the key parameters which greatly impact the nanostructure. Finally, the development of its potential application based on controllable morphologies are illustrated.

2 Different Morphologies of CeO_2

There are many methods to obtain CeO_2 micro/nanocrystals. Based on the different states of raw materials, the preparation methods are usually divided into three categories: gas-phase method, liquid-phase method and solid-phase method. For gas-phase method, the defect is that the reactants are gaseous and difficult to control, the reaction needs to be completed quickly at a high temperature, and the reaction material molecules need to be mix equably in short time, which leads to expensive equipment, complex operation, poor popularity. As for the solid-phase method, the synthetic crystal size is relatively large, the morphology is irregular, and the purity is not high. So, the research of solid-phase method is not popular than liquid-phase method. The liquid-phase method is widely used to synthesise nano powders for the merits of simple device, without high vacuum, single crystal forms, low agglomeration and easy to realize industrialization. The hydrothermal method is one of the important ways to synthesize nano-CeO_2 in liquid-phase method and is widely used in preparing nano-materials with various morphologies. The principle of hydrothermal method is to prepare oxide or compound powder under high temperature and pressure in a sealed reaction kettle, usually in the condition of the water.

In the hydrothermal condition, water acts as a solvent and mineralization agent, which can participate in the reaction as a chemical component and accelerate the occurrence of chemical reaction, and increase the solubility of the substance as well. The synthesis and modification of inorganic compounds can be achieved by controlling physical and chemical factors. Compared with other preparation methods, the hydrothermal method has the unique advantages of low energy consumption, high purity, less agglomeration and controllable morphology. Different morphologies can be obtained by adjusting experiment conditions, such as the hydrothermal time, the hydrothermal temperature, the concentration of reactants, etc.

During past years, many efforts have been made to prepare CeO_2 with different morphologies [16–19]. Up to today, a variety of CeO_2 micro/nanostructure with different morphologies have been synthesised by researchers, and it can be classified based on dimensionalities of nanostructures. Here, we sum up a series of CeO_2 with different morphologies from different dimensionalities (0-D, 1-D, 2-D and 3-D).
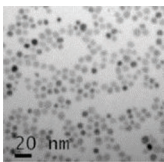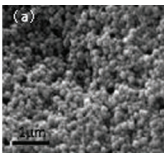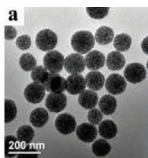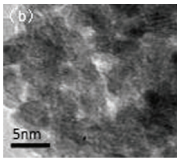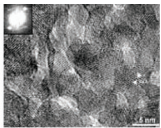
2.1 0-D Morphology

In physics, there is a zero-dimensional semiconductor structure called a quantum dot. Everything, no matter how big or small, has a certain size, when the electrons are squeezed so tightly that there is no

room to move, a zero-dimensional charge trap is formed, and the electrons trapped in this trap behave in strange but useful way. Any energy injected into a quantum dot cannot be used to transfer electrons, but can only be released as light, which makes quantum dots an efficient and low-power source. The zero dimensional CeO_2 is a particle of such a structure.

In the past decades, 0-D semiconductor quantum dots have aroused a wide concern and extensively used in the field of photocatalysts, photovoltaic device, photodetectors and phototransistors [20,21]. Usually, CeO_2 quantum dots own good photocatalytic activity for the small-size effect, and the higher quantum confinement can gain more opportunity to connect with other atoms in a heterostructure system, which lead the two components forming a closely contacted interface. Generally speaking, 0-D CeO_2 was composed of aggregated particles of 5–130 nm and the Synthesis of 0-D CeO_2 nanostructure can be summarized in Tab. 1. (Abbreviation in the table: polyvinylpyrrolidone (PVP), ethylene glycol (EG)) Typically, the 0-D CeO_2 nanoparticles mainly expose {111} planes which showed less activity for CO oxidation than other active planes [22,23].

Table 1: Summary of the 1-D morphologies and the main synthetic process of CeO_2 samples

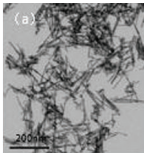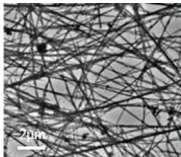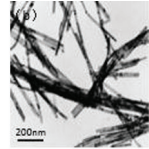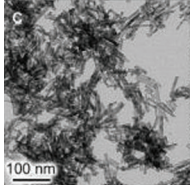| Morphology and Reactants	Main synthetic process	Images	Exposed facet	Ref.
Nanosparticles 0.5 mmol $(NH_4)_2Ce(NO_3)_6$ 1.5 mmol oleylamine 1.5 mmol Oleic acid 10 ml diphenyl ether 30 ml ethanol	1. Mixed under N_2 with magnetic stirring. 2. Heat to 180°C for 2 h. 3. Cooled down to room temperature, add 30 ml ethanol 4. Centrifugation at 8000 rpm for 8 min.	 Size: 4 nm	(200) (111)	[24]
Nanospheres 25 mmol $(NH_4)_2Ce(NO_3)_6$ 0.16 mol **PVP** 30 ml **EG**	1. Dissolve 2. Heat under reflex: 197°C, 4 h 3. Centrifuge and wash: deionized water and absolute ethanol 4. Dry: 80°C 5. Calcine: 600°C, 4 h	 Diameter: 80-100 nm	{111}	[25]
Mesoporous spheres 2.3 mmol $Ce(NO_3)_3·6H_2O$ 1 ml H_2O 1 ml C_2H_5COOH 30 ml glycol	1. Dissolve 2. Heat: 180°C 200 min	 Diameter: 130 nm	(111)	[26]
Nanoparticles 1 mmol $(NH_4)_2Ce(NO_3)_6$ 0.03 mol $CO(NH_2)_2$ 20 ml H_2O	1. Dissolve 2. Heat under stirring: 80°C, 27 h 3. Filtration and wash: deionized water 4. Dry: 100°C, 12 h 5. Calcine: 400°C, 5 h, air	 Average size: 6 nm	{111}	[27,28]
Nearly sphere Ce powders (5 μm) high-energy attritor ball mill	Ball to powder ration of 40:1 Angular speed: 400 rpm for 10 to 50 h in dry medium	 Average size: ~10 nm	(001)	[29]

As shown in Tab. 1, CeO_2 nanospheres, mesoporous spheres and nanoparticles can be prepared via a simple solution route. Usually, it is hard to control homogeneity of the particle size when synthesised the quantum dots. When Imagawa et al. [24] synthesised the 4 nm ceria nanoparticles, they use the oleylamine and Oleic acid as surfactants, the binding between Oleic acid and Ce-ion might facilitate CeO_2 nucleation in diphenyl ether, which lead to form the smaller CeO_2 nanoparticles [30,31]. What's more, the suitable nucleation temperature can help to develop more uniformed size and shape. Therefore, the reaction temperature needs to be controlled precisely. Similarly, they also synthesised 6 nm CeO_2 nanoparticles. The annealed CeO_2 nanoparticles are active for oxygen storage and release, the small nanoparticles show a high oxygen storage capacity [32–34]. The mesoporous spheres are made up of lot of small particles with a crystallite size of 3–5 nm. Attractively, there are voids with a diameter of 3–5 nm among these nanoparticles which help to improve the specific surface area. In this way, it might be an excellent candidate applied in catalysis.
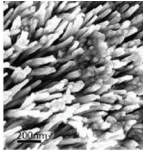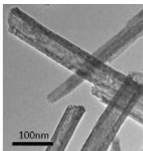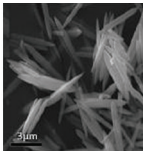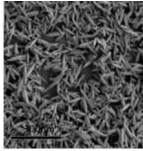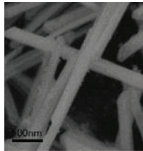
2.2 1-D Morphology

Compared with 0-D CeO_2, the morphologies and structure of 1-D CeO_2 are rather prolific. 1D CeO_2 was hexagonal rods that were 25–30 μm in width and more than 500 μm in length.

A serious of 1-D CeO_2 nanostructure have been realized successfully till now. The synthesis of 1-D CeO_2 can be summarized in Tab. 2. (Abbreviation in the table: polyvinylpyrrolidone (PVP), ethylene glycol (EG))

Table 2: Summary of the 1-D morphologies and the main synthetic process of CeO_2 samples

Morphology and Reactants	Main synthetic process	Images	Exposed facet	Ref.
Nanowires 1.9 mmol $Ce(NO_3)_3 \cdot 6H_2O$ 0.4 mol NaOH 80 ml H_2O	1. Dissolve 2. Heat: 100°C, 14 h 3. Wash: hot water 4. Dry: 100°C, over night 5. Calcine: 400°C, 4 h, air	Length: ~140 nm Diameter: ~7 nm	{110} {100}	[28]
Nanowires 0.675 mmol $CeCl_3 \cdot 7H_2O$ 0.09 mol NaOH 8.9 mmol NaCl 15 ml H_2O	1. Dissolve 2. Heat: 180°C, 24 h 3. Centrifuge and wash: deionized water 4. Dry: 200°C, overnight 5. Calcine: 600°C, 3 h	Length: 1-3 μm width: 20-60 nm	(110)	[35]
Nanorods 1.8 mmol $CeCl_3 \cdot 7H_2O$ 0.27 mol NaOH 30 ml H_2O	1. Dissolve 2. Heat: 140°C, 48 h 3. Centrifuge and wash: wash with deionized water to neutrality, then wash with ethanol several times. 4. Dry: 60°C, overnight, air	Length: 50-125 nm Diameter: 25-45 nm	(111) (110) (100)	[37]
Nanorods 6.9 mmol $Ce(NO_3)_3 \cdot 6H_2O$ 0.16 mol NaOH 80 ml H_2O	1. Dissolve 2. Heat: 100°C, 14 h 3. Wash: hot water 4. Dry: 100°C, overnight 5. Calcine: 400°C, 4 h	Length: 60-120 nm Diameter: 7-15 nm	(110)	[28]

Table 2 (continued).

Morphology and Reactants	Main synthetic process	Images	Exposed facet	Ref.
Nanorods array 3 mmol $Ce(NO_3)_3 \cdot 6H_2O$ 0.15 mmol $Na_3PO_4 \cdot 6H_2O$ 40 ml H_2O	1. Dissolve 2. Heat: 220°C, 12 h 3. Centrifuge and wash: deionized water and absolute ethanol 4. Dry: 60°C, air	Length: several µm Diameter: 30 nm	(100)	[37]
Nanotubes Step 1: 3.9 mmol $Ce(NO_3)_3 \cdot 6H_2O$ 0.06 mol $CO(NH_2)_2$ 80 ml H_2O Step 2: As-prepared $Ce(OH)CO_3$ Adequate NaOH	Step 1: stirring hydrothermal process 1. Dissolve 2. Heat under stirring: 80°C, 24 h 3. Centrifuge and wash: distilled water 4. Dry: 60°C → obtain $Ce(OH)CO_3$ Step 2: hydrothermal process 1. Dissolve 2. Heat: 120°C, 24 h 3. Wash: distilled water and ethanol 4. Dry: overnight, vacuum	Outer diameter: 20-45 nm Inner diameter: 10-25 nm	(111)	[38–40]
Spindle-like 0.025 $mol(NH_4)_2Ce(NO_3)_6$ 0.16 mol PVP 30 ml EG	1. Dissolve 2. Heat under reflex: 197°C, 24 h 3. Centrifuge and wash: deionized water and absolute ethanol 4. Dry: 80°C 5. Calcine: 600°C, 4 h	Diameter: Several hundred nm	(111)	[25]
Shuttle-like 2 mmol $Ce(NO_3)_3 \cdot 6H_2O$ 4 mmol $CO(NH_2)_2$ 40 ml H_2O	1. Dissolve 2. Heat: 150°C, 24 h 3. Centrifuge and wash: distilled water and ethanol 4. Dry: 70°C, 12 h 5. Calcine: 600°C, 4 h	Diameter: 16 nm	(111)	[41]
Nano hexagonal prisms 1.15 mmol $Ce(Ac)3 \cdot nH_2O$ 10 mol NaOH 20 ml H_2O	1. Dissolve 2. Heat: 200°C, 24 h 3. Wash: distilled water 4. Dry: 70°C, 8 h	Diameter: 100-250 nm	(220) (111)	[42]

As shown in Tab. 2, shape-controlled synthesis of the 1-D CeO_2 nanostructure has been realized by our researchers. Changing reaction conditions can synthesize various structures. As the table shown, we can get nanowires, nanorods, nanotubes, nano hexagonal prisms and so on when under different heating, calcining or drying temperature and duration. From another perspective, it is evident that discrepant reaction conditions will synthesize the same nanostructure with different sizes. For instance, Tana et al. [28] and Ke et al. [35] used different cerium precursor to synthesize CeO_2 nanowires via a hydrothermal method, and the size of nanowires fabricated by Ke et al. are larger, but both arrangement of the nanowires are chaotic. Subsequently, the ordered ceria nanowire crystals were further arranged by La et al. [43] via an

electrochemical method. Furthermore, different structures can even be transformed under certain conditions, like the 0-D to 1-D. In conclusion, by changing reaction reactants or parameters can synthesize the same structure with different size or different kinds of the nanostructure.
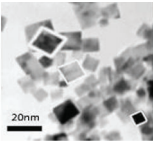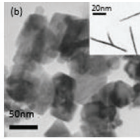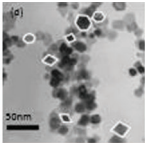
The CeO_2 nanotubes was reported by Li et al. [38] They synthesised the CeO_2 nanotubes in two steps [39]. The first step is based on the work finished by Chen et al. [40], which through a series of chemical reactions to obtain the $Ce(OH)CO_3$ precursor. Then the second step was a hydrothermal treatment of as-prepared $Ce(OH)CO_3$ precursor and NaOH solution. Finally, the CeO_2 nanotubes was successfully fabricated. What is more, CeO_2 nanotubes can be successfully prepared by one-step process as well. Gonzalez-Rovira et al. [44] used the electrodeposition method to manufacture triumphant CeO_2 nanotubes via a single-step process.
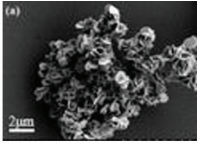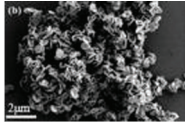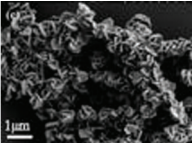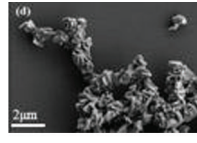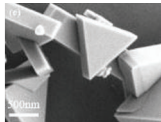
The method of synthesizing CeO_2 spindle-like nanostructure is similar to the method used by Ho et al. [25] to prepare CeO_2 nanospheres. As shown in Tabs. 1 and 2, the only difference is that they prolong the reflux time to 24 h. Accordingly, the CeO_2 nanospheres were gradually evolved into the spindle-like nanostructure. The formed spindle-like particles are hundreds of nanometers wide, and aspect ratio is about 4–8. The detail synthesize parameters of shuttle-like structure and nano hexagonal prisms can be seen in Tab. 2.

2.3 2-D Morphology

2-D nanomaterials are particularly attractive in recent years for their high surface-to-volume ratio, high crystallinity, potential quantum size effects and explicit chemical composition as well as extremely high anisotropy with an ultrathin thickness [45–49]. Based on these benefits, there is great potential for development in the field of modern high technology, like automobile emission purification, high-temperature photosensitive materials, etc. However, the synthesis of 2-D CeO_2 structure is rarely reported for lack of intrinsic driving force for 2-D anisotropic growth. in this way, it is much more difficult to control the crystal growth in two dimensions. Here, we summarize the Synthesis route of 2-D CeO_2 in Tab. 3.

Table 3: Summary of the 2-D morphologies and the main synthetic process of CeO_2 samples

Morphology and Reactants	Main synthetic process	Images	Exposed facet	Ref.
Nanoplates (cubic) 3 mmol $Ce(NO_3)_3 \cdot 6H_2O$ 2 mmol CTAB 4 ml $NH_3 \cdot H_2O$	1. Dissolve 2. Heat: 100°C, 24 h 3. Wash: deionized water 4. Dry: 80°C, 24 h	Crystallite size: ~17 nm Thickness: ~3 nm	(100)	[50]
Nanoplates (irregular) 3 mmol $Ce(NO_3)_3 \cdot 6H_2O$ 2 mmol CTAB 4 ml $NH_3 \cdot H_2O$	1. Dissolve 2. Heat: 120°C, 24 h 3. Wash: deionized water 4. Dry: 80°C, 24 h	Crystallite size: ~40 nm Thickness: ~3 nm	(100)	[35]
Nanoplates (rhombic and hexagonal) 3 mmol $Ce(NO_3)_3 \cdot 6H_2O$ 2 mmol CTAB 4 ml $NH_3 \cdot H_2O$	1. Dissolve 2. Heat: 160°C, 24 h 3. Wash: deionized water 1. Dry: 80°C, 24 h	Crystallite size: ~15 nm Thickness: ~3 nm	(111)	[35]

Table 3 (continued).

Morphology and Reactants	Main synthetic process	Images	Exposed facet	Ref.
Nanosheets (disk-like polygonal) 4 mmol $CeCl_3 \cdot 7H_2O$ 0.04 mol NH_4HCO_3 10 ml $C_2H_8N_2$ 25 H_2O	1. Dissolve 2. Heat: 160°C, 48 h 3. Wash: deionized water and ethanol 4. Dry: 60°C, 12 h 5. Calcine: 500°C, 5 h, air	Diameter: 0.8-1.3 μm Thickness: 50-100 nm	{111}	[51]
Nanosheets (hexagonal) 4 mmol $CeCl_3 \cdot 7H_2O$ 0.04 mol NH_4HCO_3 10 ml $C_2H_8N_2$ 25 H_2O	1. Dissolve 2. Heat: 180°C, 48 h 3. Wash: deionized water and ethanol 4. Dry: 60°C, 12 h 5. Calcine: 500°C, 5 h, air	Edge length: 300-400 nm Thickness: 40-50 nm	{111}	[36]
Nanosheets (triangular outline) 4 mmol $CeCl_3 \cdot 7H_2O$ 0.04 mol NH_4HCO_3 10 ml $C_2H_8N_2$ 25 H_2O	1. Dissolve 2. Heat: 190°C, 48 h 3. Wash: deionized water and ethanol 4. Dry: 60°C, 12 h 5. Calcine: 500°C, 5 h, air	Edge length: 400-500 nm Thickness: ~100 nm	{111}	[36]
Nanosheets (regular triangular) 4 mmol $CeCl_3 \cdot 7H_2O$ 0.04 mol NH_4HCO_3 10 ml $C_2H_8N_2$ 25 H_2O	1. Dissolve 2. Heat: 200°C, 48 h 3. Wash: deionized water and ethanol 4. Dry: 60°C, 12 h 5. Calcine: 500°C, 5 h, air	Edge length: 0.5-1 μm Thickness: 50-150 nm	{111}	[36]
Nanosheets (perfect triangular) 4 mmol $CeCl_3 \cdot 7H_2O$ 0.04 mol NH_4HCO_3 10 ml $C_2H_8N_2$ 25 H_2O	1. Dissolve 2. Heat: 220°C, 48 h 3. Wash: deionized water and ethanol 4. Dry: 60°C, 12 h 5. Calcine: 500°C, 5 h, air	Edge length: 1-2 μm Thickness: 300-400 nm	{111}	[36]

CeO_2 nanoplates was reported by Ke et al. [35] for the first time via a hydrothermal condition which was assisted by CTAB and the brief synthesis route is shown in Tab. 3. Besides, when adjusting the hydrothermal temperature, a series of nanoplate morphologies will be produced. This is because the face-centered cubic ceria crystal mainly exposed facet (100) and (111) [52,53]. When the hydrothermal temperature is low, the CTAB may absorb on the exposed facet (100) of ceria crystal and limits to grow which lead the crystal shape to become cubic. However, when improved the hydrothermal temperature, the shape of the crystal self-assembled by plane (111) is rhombic or hexagonal. To be specific, the nanoplate is mostly cubic at 100°C, however, it takes on an irregular shape at 120°C. As the temperature increases to 140°C, the ratio of irregular plates correspondingly decreases; nevertheless, the trend of the rhombic and hexagonal plates are going in the same direction with the temperature. Until up to 160°C, the rhombic

and hexagonal plates predominate in the products, with few irregular plates. On the other hand, the size of nanoplates increases firstly and then decreases with the temperature rising after the peak. It is worth mentioning that the parameters at the vertex depend on the reaction conditions and the type of reactant.

CeO_2 nanosheets have been successfully synthesized by Gong et al. [51] via a facile hydrothermal treatment. They used $CeCl_3 \cdot 7H_2O$ as Cerium source to synthesize the CeO_2 nanosheets, and the brief synthesis process is covered in Tab. 3. According to the table above, we can find that by changing different hydrothermal temperature, a serious of different morphologies of CeO_2 nanosheets can be obtained and they mainly exposed {111} crystal plane with the temperature improving, the shape of nanosheets becomes more and more regular and finally becomes perfect triangular. Meanwhile, the thickness of the nanosheets goes up steadily and the size of nanosheets decreases initially but increases subsequently after the peak, there is an inflection point in the whole trend.

2.4 3-D Morphology

Three dimensions, by definition, have length measures in three directions. 3-D CeO_2 mainly contains nano-cubes, nano-octahedrons and flower-like structures. In addition to the above mentioned, there are others that apply to specific structures in specific situations, also attracting much attention because of their unique properties and potential applications [54–56]. The synthesis of 3-D CeO_2 can be summarized in Tab. 4. (Abbreviation in the table: tetrabutylammonium bromide (TBAB), ethylene glycol (EG)).

Table 4: Summary of the 3-D morphologies and the main synthetic process of CeO_2 samples
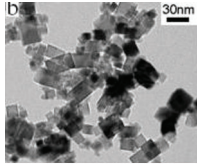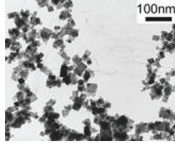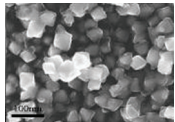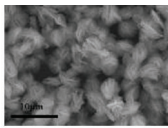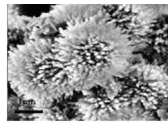
Morphology and reactants	Main synthetic process	Images	Exposed facet	Ref.
Nano-cubes 1.8 mmol $Ce(NO_3)_3 \cdot 6H_2O$ 0.27 mol NaOH 30 ml H_2O	1. Dissolve 2. Heat: 140°C, 48 h 3. Centrifuge and wash: wash with deionized water to neutrality, then wash with ethanol several times. 4. Dry: 60°C, overnight, air	 Size: 8-30 nm	{100}	[36]
Nano-cubes 1.8 mmol $CeCl_3 \cdot 7H_2O$ 0.27 mol NaOH 30 ml H_2O 5.4 mmol $NaNO_3$	1. Dissolve 2. Heat: 140°C, 48 h 3. Centrifuge and wash: water and ethanol 4. Dry: 60°C, overnight 5. Calcine: 400°C, 4 h	 Size: ~20 nm	{100}	[36]
Nano-cubes 2 mmol $Ce(NO3)_3 \cdot 6H_2O$ 0.24 mol NaOH 40 ml H_2O	1. Dissolve 2. Heat: 100°C, 24 h 3. Centrifuge and wash: water and ethanol 4. Dry: 60°C, overnight 5. Calcine: 400°C, 4 h	 Size: 10-37 nm	(100) (110)	[57]
Nano-octahedrons 1 mmol $Ce(NO_3)_3 \cdot 6H_2O$ 0.01 mmol $Na_3PO_4 \cdot 6H_2O$ 40 ml H_2O	1. Dissolve 2. Heat: 170°C, 12 h 3. Centrifuge and wash: deionized water and ethanol 4. Dry: 60°C, 24 h	 Edges lengths: ~100-200 nm	{111}	[58]

Table 4 (continued).

Morphology and reactants	Main synthetic process	Images	Exposed facet	Ref.
Flowerlike structure 4 mmol CeCl$_3$·6H$_2$O 0.037 CO(NH$_2$)$_2$ 0.019 TBAB 150 ml EG	1. Dissolve 2. Heat under stirring: 170°C, 30 min 3. Centrifuge and wash: ethanol 4. Calcine: 450°C, 2 h	Diameter: ~4-6 μm	(111)	[59]
Flowerlike nanorods 7.5 mol Ce(NO$_3$)$_3$·6H$_2$O 0.37 mmol Na$_3$PO$_4$·6H$_2$O 40 ml H$_2$O	1. Dissolve 2. Heat: 220°C, 12 h 3. Centrifuge and wash : deionized water and absolute ethanol 4. Dry: 60°C, air	Diameter: ~2-4 μm	(200)	[37]

As shown in Tab. 4, Wu et al. [36] used Ce(NO$_3$)$_3$·6H$_2$O as the cerium source to synthesize CeO$_2$ nanocubes, which synthetic procedure was similar to nanorods. What we should pay attention is that they used CeCl$_3$·7H$_2$O as the cerium source and adding a certain amount of NaNO$_3$ into the hydrothermal solution, which is also the attraction in this experiment. Accordingly, CeO$_2$ nanocubes could also be synthesized by a similar synthetic route. Lee et al. [57] and He et a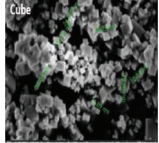l. [42] also synthesized CeO$_2$ nanocubes via an analogous method as Wu et al. But the difference is that He et al. increased the size of nano-cubes to several hundred nm. Cubic cerium oxide owns fabulous catalytic activity in most of the chemical reaction, owning to its intrinsic properties, such as the high mobility and oxygen storage capacity within the lattice and the valence state of cerium can easily changes between Ce^{3+} and Ce^{4+} [60,61].

The synthetic route of CeO$_2$ nano-octahedrons, flowerlike structure and flowerlike nanorods can be observed in this table as well. Yu et al. [37] use an akin hydrothermal method to synthesize ceria flower-like nanorods as they used to synthesize nanorods arrays. The only change is that they improved the concentration of Ce(NO$_3$)$_3$·6H$_2$O to a suitable value. In this way, ceria flower-like nanorods were successfully fabricated. The flower-like nanostructure manufactured is composed of lots of nanorods, and the diameter of each nanorod is about 20–40 nm while the length is about 1–2 μm.

Besides, apart from the kind of 3-D structure is more abundant, and the size of that is larger, we can discover that the heat temperature 3-D needed is higher when compared with other CeO$_2$ nanostructures. To account for this phenomenon, we believe that this is related to the temperature required for the grain to grow to higher dimensions.

Until now, the preparation methods mainly include precipitation method, sol-gel method, combustion method and hydrothermal method. Among the different synthesis methods, precipitation method is the relatively popular one with researchers on account of its simple equipment and controllable process. Recently, combustion method has gained much more attention compared with other methods. However, the combustion method also has some drawbacks. The reaction is that it is carried out under high temperature and high pressure, which requires strict requirements on experimental equipment and requires large investment. Sol-gel method is a common method for preparing nano-metal oxide particles at low temperature, with the merit of high in purity and good dispersity. Whereas, using this method, the reaction time is long, the sample is easy to agglomerate and the raw material cost is high.

3 Effect of Reaction Conditions on CeO$_2$ with Different Morphologies

According to the experiments and corresponding analyses finished by researchers in this field, some interesting conclusions can be summed up when synthesizing the CeO$_2$ nanostructure via a solution route.

3.1 The Concentration of Reactants

The concentration of reactants plays an important part in the formation and growth of CeO_2 grains. For instance, Yu et al. [37] used $Ce(NO_3)_3 \cdot 6H_2O$ and $Na_3PO_4 \cdot 6H_2O$ (the molar ratio of PO_4^{3-} to Ce^{3+} was kept at 5%) as reactants to synthesize CeO_2 nanostructure. To be specific, when the concentration of $Ce(NO_3)_3 \cdot 6H_2O$ is set as 0.025 M, the morphologies are nano-octahedrons and nanorods. When they improved the concentration to 0.05 M, only obtained nanorods morphology. What's more attractive is that the verticality aligned nanorods were successfully obtained when they increase the concentration to 0.1 M, at the same time, the diameter of nanorods gets a little bigger. Finally, when the concentration is increased to 0.25 M, the flower-like nanorods were obtained. Fig. 1 shows the FE-SEM images of CeO_2 nanostructure fabricated by hydrothermal treatment with different cerium ion concentration. It is interesting to see that the morphology of CeO_2 changed with the increase of Ce^{3+} concentration.
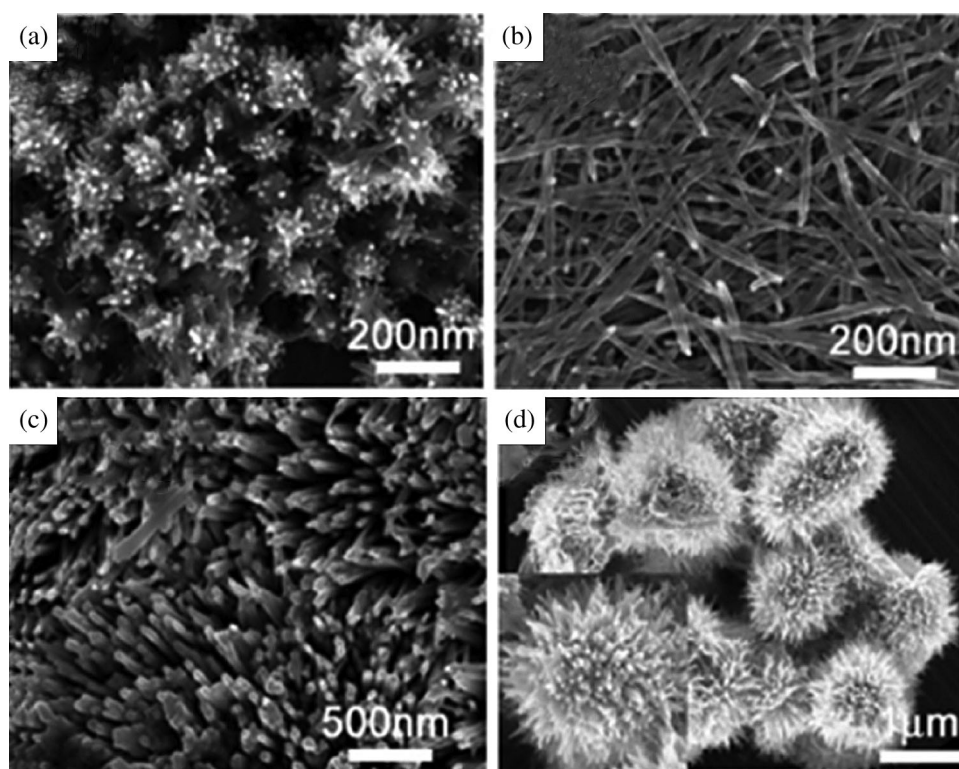
Figure 1: FE-SEM images of CeO_2 nanostructure obtained by hydrothermal treatment with cerium ion concentration of (a) 0.025 M; (b) 0.05 M; (c) 0.1 M; (d) 0.25 M at 220°C. Adopted from Yu et al. [37], Copyright 2008 American Chemical Society

It is natural to find that if we keep other parameters the same and change the concentration of reactants, the morphology will change correspondingly. When the concentration of Ce^{3+} is low, increasing the concentration of Ce^{3+} can improve the supersaturation of solution, which assists the nucleation of the crystal. The supersaturation will vanish before the nucleus growing up, so the size of obtained CeO_2 nanostructure is small. When the concentration of Ce^{3+} is too high, the thermodynamic factors will become the lead factor which will appear self-aggregation for the reason that the Gibbs free energy is less than zero in the sedimentation process.

Yan et al. [58] use the same reactants to synthesize CeO_2 nanostructure, they also found that the concentration of PO_4^{3-} was a dominant factor to form the CeO_2 nanostructure. When the concentration of PO_4^{3-} was less than 1×10^{-4} M, only a large amount of mixed morphology of octahedron and rod-like structure could be obtained rather than uniform nano-octahedron and nanorods. Only make the phosphate ions concentration within bounds can obtain the uniform nano-octahedron and nanorods.

Based on the experiments and analysis, Yu et al. [37] found that there is a correlation between the effect of phosphate and cerium ion concentration on the morphology of CeO_2. But how does the phosphate group control CeO_2 morphologies? After a series of research, they find that the phosphate group may affect the surface electrostatic potential and energy of nanorods, and further control the CeO_2 morphologies. When the Ce^{3+} concentration is low, the low CeO_2 yield lead to the morphology control effect of phosphate groups was inconspicuous, and the growth of CeO_2 crystal had a lower orientation. And when the Ce^{3+} concentration of was increased to a range value, the nanorods would rearrange into vertically well-aligned nanorods hierarchical architectures which assist by the high electrostatic potential and surface energy on CeO_2 surface. Finally, when the concentration of Ce^{3+} increasing to a certain value, the surface energy of CeO_2 would decrease, which lead the nanorods arise self-aggregation to form the flower-like nanorods. Other researchers also proved that the concentration of reactants have an important impact on the formation of CeO_2 nanostructure, not go into detail here.

3.2 The Hydrothermal Temperature

What's more, the hydrothermal temperature has a significant impact on the formation of the CeO_2 micro/nano structure. Yu et al. [37] have studied the effect of hydrothermal temperature on morphology as well. When they use $Ce(NO_3)_3 \cdot 6H_2O$ and $Na_3PO_4 \cdot 6H_2O$ to synthesize CeO_2 nanostructure, the hydrothermal temperature was set as the only variable and keep other factors the same. The concentration of Ce^{3+} is set as 0.1 M and reaction time is 12 h, only change the temperature. As shown in Fig. 2, a mixed morphology of nanoparticles and nanorods were obtained at 140°C. when increasing the temperature to 170°C, 1-D nanorods morphology can be obtained. Further increasing the hydrothermal temperature to 220°C can form the vertical nanorods arrays. So, we can see that a higher temperature can assist the formation of 1-D morphology and further increase the temperature to a suitable value can form ordered nanorods arrays.
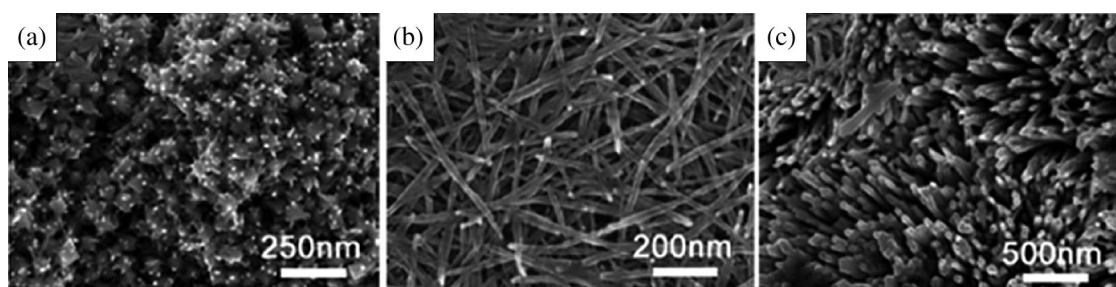
Figure 2: FE-SEM images of CeO_2 nanostructure obtained by hydrothermal treatment for 12 h with cerium ion concentration of 0.1 M at (a) 140°C; (b) 170°C; (c) 220°C. Adopted from Yu et al. [37], Copyright 2008 American Chemical Society

Pan et al. [62] use $Ce(NO_3)_3 \cdot 6H_2O$ and NaOH as reactants to fabricate CeO_2 nanostructure and find that hydrothermal temperature can assist CeO_2 form different morphologies. They set reaction temperature at 110°C, 120°C, 140°C, 160°C, 180°C, keep other parameters the same (the detail condition is covered in reference), an attractive morphologies conversion can be realized. as shown in Fig. 3, with the temperature gradually increasing, nanowires convert into nano-cubes, and the size of nano-cubes get

larger gradually. So, we can conclude that the hydrothermal temperature may affect the recrystallisation and grain growth of CeO_2 nanostructure, the different temperature may offer suitable growth condition to form different morphologies.
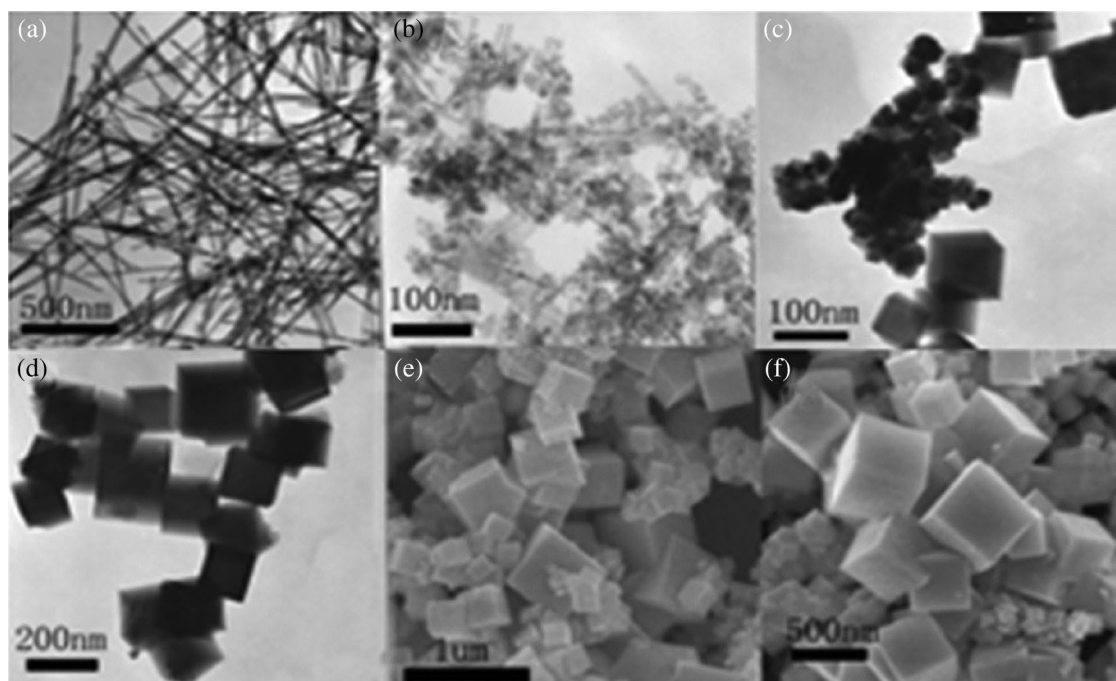
Figure 3: TEM images of CeO_2 nanostructure obtained by hydrothermal treatment for 24 h with cerium ion concentration of 0.4 M at (a) 110°C; (b) 120°C; (c) 140°C; (d) 160°C; (e) 180°C; (f) 180°C. Adopted from Pan et al. [62], Copyright 2008 Wiley-VCH Verlag GmbH & Co. KGaA, Weinheim

3.3 The Hydrothermal Time

The hydrothermal time can influence the formation of CeO_2 nanostructure as well. Yan et al. [58] find that prolong the hydrothermal time can assist the nano-octahedrons convert into nanorods, as shown in Fig. 4. When reaction time prolongs to 24 h, the 1-D nanorods began to grow up out of the octahedrons surface and became more and more longer. Finally, when increasing time to 144 h, almost all the nano-octahedrons convert into nanorods. They use a nucleation-dissolution-recrystallization mechanism [63] to express the formation of multiple nano-structures and morphology evolution from nano-octahedron to nanorods, as shown in Fig. 5. In the beginning, the irregular shapes of the CeO_2 nanocrystals were formed in the solution via a homogeneous nucleation process. After that, the as-obtained nanoparticles begin to agglomerate and then self-assemble to form nano-octahedrons. When further increased hydrothermal time, it was observed that there were many small protuberances on the surface of the nano-octahedrons, which provided many high-energy sites for nanocrystal growth [64]. Thus, the small protuberances may provide the active site for the nucleation of dissolved CeO_2 in the solution, which lead the CeO_2 grow along the 1-D direction and recrystallize into nanorods until the CeO_2 nano-octahedrons completely dissolved.

Pan et al. [50] also find that change the hydrothermal time can influence the formation of the CeO_2 nanostructure. As shown in Tab. 3, the morphologies of CeO_2 nanoplates changed with changing the reaction time. Other experiments data will not mention in detail here.
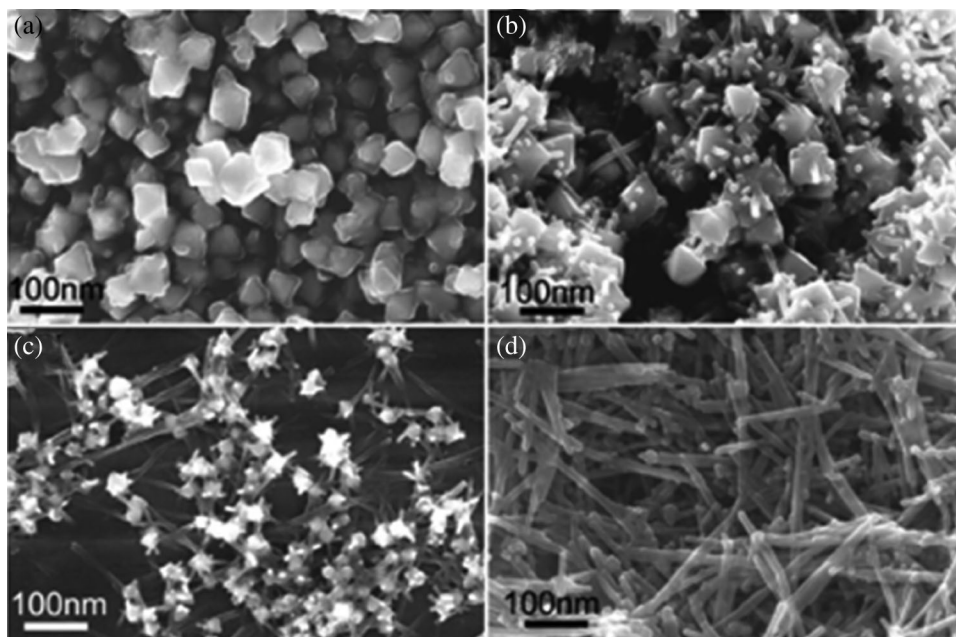
Figure 4: FE-SEM images of CeO_2 nanostructure hydrothermal treated at 170°C for (a) 12, (b) 24, (c) 48, (d) 144 h. Adopted from Yan et al. [58], Copyright 2008 American Chemical Society
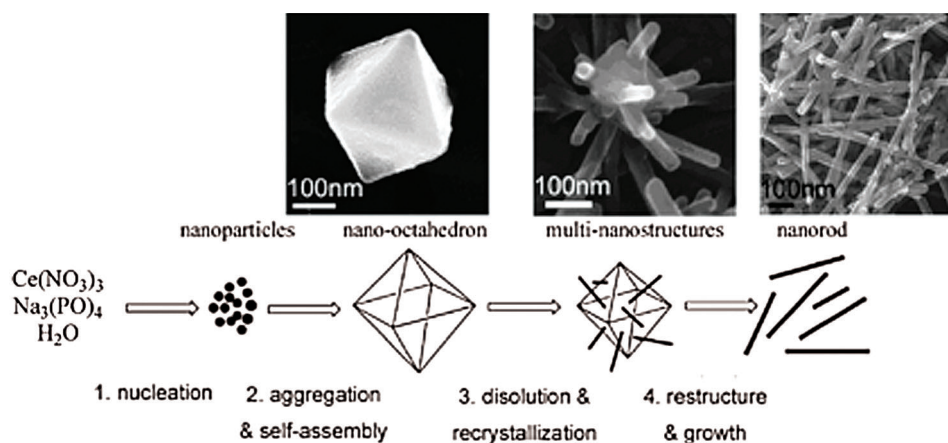
Figure 5: Schematic illustration for the multiple nano-structures evolution of CeO_2. Adopted from Yan et al. [58], Copyright 2008 American Chemical Society

3.4 The Cerium Precursor

Finally, it can be concluded that different cerium precursor can influence the morphologies of CeO_2 nanostructure for the reason that anions may influence its nucleation and growth. Based on summarizing a large amount of literature, we find that the anions Cl^- and Ac^- helps to synthesize nanowire, nanorods and nano hexagonal prisms while the oxidizing anions NO_3^- accelerate the formation of nano-cubic. As Fig. 6 shows, different anions can assist the formation of different CeO_2 nanostructure. It is also found that the counter-anions of the cerium source were significant to the shape of the resulting products. And it is proved that nanorods could be fabricated when the counter-anions are Cl^- Br^- I^- SO_4^{2-} ions, and irregular nanoparticles are produced when the counter-anions is BrO_3^- ions.
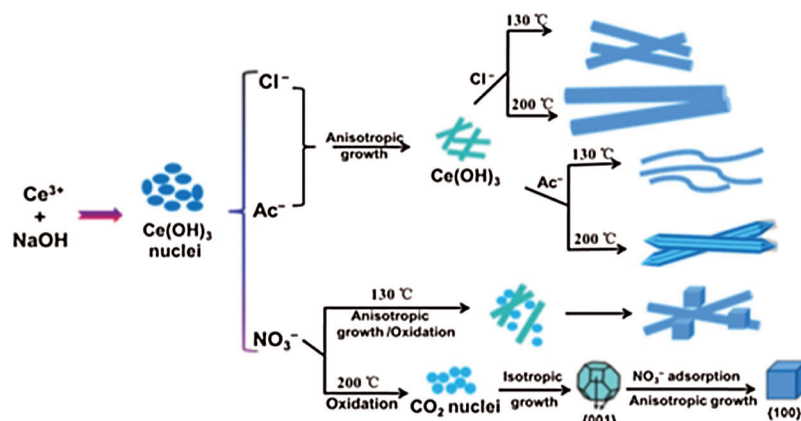
Figure 6: Schematic diagram for the formation process of the different CeO_2 nanostructure. Adopted from He et al. [42], Copyright 2016 Elsevier Ltd. and Techna Group S.r.l

In conclusion, these factors play crucial parts in the formation of different CeO_2 nanostructure, and there are some other factors that may influence the shapes of CeO_2 as well. Sometimes one specific shape can be obtained by adjusting different factors. Because this specific shape is a combination of various factors, it is hard to clear the influence of a specific factor.

4 Applications

CeO_2 has become one of the most important rare earth materials because of CeO_2 is widely used in redox reactions due to its superior oxygen storage function and high temperature and rapid oxygen vacancy diffusion capacity [65]. What is more important is that the unique chemical, mechanical, electrical and optical properties of Cerium dioxide nanoparticles have attracted wide-spread attention, especially when the size of it is on the nanoscale [66]. The structure dominates properties, thus, it is necessary to synthesize cerium dioxide with controllable morphologies for expressing excellent properties which is also the main technical problem. Hitherto, a variety of cerium dioxide with different micro/nano morphologies have been synthesized by researchers and it can be used to many fields according to different structure. However, the control of nanostructures remains the most important challenge we face. In other words, effective control both technically and economically of particles can help us achieve the aim of widespread use.

4.1 Application in Superhydrophobic Coatings

Fabricating a superhydrophobic surface is one of the effective means to protect or prevent the metal out of corrosion [67–69]. According to relevant research, it is proved that the main factor to generate the super hydrophobicity are chemical compositions which decide the surface free energy and the geometric structure at microscopic level which controls the surface roughness [70–74]. Superhydrophobic surface nanostructure dominates the wettability of solid/liquid contact mode and therefore plays an important role in meeting the desired water repellence. What's more attractive is that the high thermal stability and large robust nature which make the cerium dioxide be an ideal candidate for highly stable superhydrophobic material. Therefore, researchers focus much eyesight on fabricating superhydrophobic CeO_2 coatings on the metal or metal alloys surface.

A case in point is that Ishizaki et al. [75] fabricated superhydrophobic CeO_2 films on magnesium alloy in NaCl aqueous solution. The surface prepared by them showed excellent corrosion-resistant performance and durability. What's more, the superhydrophobic CeO_2 nanotube film was fabricated by Li et al. [38] showed that the water contact angle is about $157 \pm 0.6°C$ and generated a strong adhesion between the water droplet and the film, as shown in Fig. 7a. The possible reason for high water adhesion is illustrated in Fig. 7b. Correspondingly, they proved that the film of CeO_2 nanotubes can resist high temperature up to 450°C and owns long-term durability in the chemical environment, as shown in Figs. 7c and 7d.
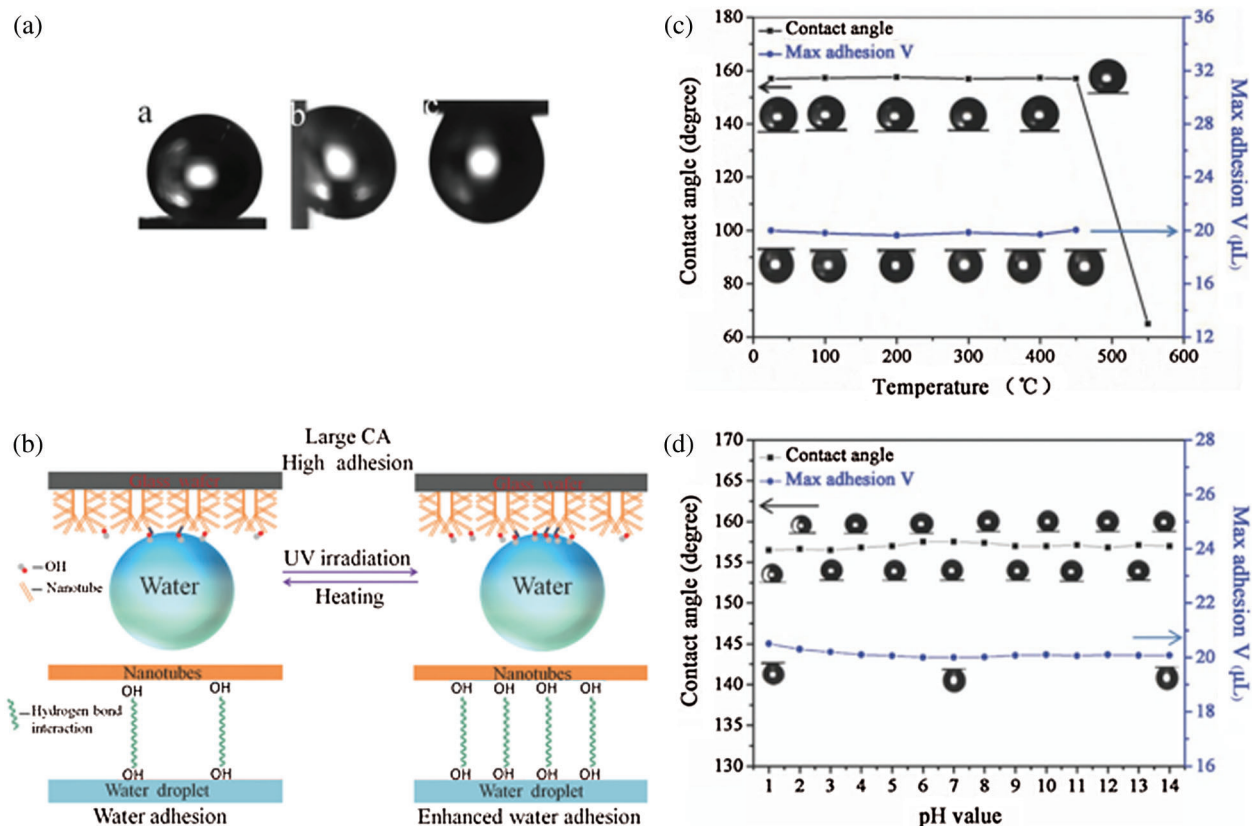
Figure 7: (a) The optical photographs for the water droplets on the newly prepared CeO_2 nanotube film under different tilt angles: (a) 0°, (b) 90°, (c) 180°. (b) Schematic illustration regulation of water adhesion over the film of CeO_2 nanotubes. (c) Effect of the temperature of heat treatment on the CA and maximum adhesion volume of water for the film of CeO_2 nanotubes. The periods of time for heat treatment at various temperatures are all 2 h. (d) Variations in the CA and maximum adhesion volume of water for the film of CeO_2 nanotubes immersed in the aqueous solutions with various pH values for 7 d. The pH value was adjusted by using diluted NaOH or HCl. Adopted from Li et al. [38], Copyright 2018 John Wiley & Sons, Inc.

The properties they have tested behaved excellently, which are very significant in practical application. Attractively, Nanorods arrays, nano-octahedron, flower-like nanorods and flowerlike structure are promising nanostructure to apply to superhydrophobic coatings for their excellent surface roughness if they can grow in metal substrate. In conclusion, CeO_2 nanostructure with different morphologies has very promising application in superhydrophobic coatings.

4.2 Application in Catalysis

Catalysis is of major socioeconomic importance for our society, it helps to solve the future problems connected with limited resources and energy. Recently, morphology engineering of catalyst nanoparticles makes it possible to tailor catalytic performance without affecting catalyst composition. What's more attractive is that well-defined particles morphologies could facilitate to establish the structure-performance relationship. The previous studies proved that the redox property of CeO_2 mainly depends on different exposed facets on the surface of the nanocrystalline [76–80]. Generally, three low-index lattice planed exist on the surface of CeO_2 nanocrystal: (100), (110) and (111), the unit cell and three low-index surface of CeO_2 structure as shown in Figs. 8a–8d, Other surfaces, such as (211), (221) and (310) are less stable and would severe reconstruction [81–84]. The property that CeO_2 easily releases and takes up oxygen makes the oxide attractive for catalytic application in which oxygen transfer reactions are involved [85–89]. It is proved that the exposure of more reactive (100) facet, followed by (100) facet, should accelerate the formation of oxygen vacancies. Thus, the nanowires, nanaorods arrays, nanoplates, nanocubes and flower-like nanorods owns favorable oxygen storage capacity. Fig. 8e shows the cubic fluorite structure of CeO_2 along with oxygen vacancy and Ce^{3+} in the lattice site [90]. They proved that adjusting the formation of the oxygen vacancy in CeO_2 is necessary to make it more efficient for application in catalysis. González-Rovira et al. [91] used a single-step process to prepare CeO_2 nanotubes with improved catalytic activity. Fig. 8f shows the light-off curve of CeO_2 nanotubes and powder CeO_2. it is found that the CeO_2 nanotubes with exposed {100} facets Showed a favorable catalytic activity in CO oxidation, which is approximately 400 times higher than powdered CeO_2 at 200°C. Liang et al. [26] have studied the catalytic performance of CeO_2 in CO oxidation reaction as well. The conversion profiles of CO versus temperature reveals the excellent catalytic performance of the CeO_2 mesosphere. In addition, Tana et al. [28] have studied the catalytic activities of CeO_2 nanowires, nanorods and nanoparticles for CO oxidation, the CO conversion curve is showed in Fig. 8g. It shows that CeO_2 nanowires are more active than the CeO_2 nanorods and nanoparticles, whereas, both CeO_2 nanowires and nanorods mainly expose the {110} and {100} planes, the reason why the CeO_2 nanowires behave more active is that the nanowire expose most of these active planes on the surface. The CeO_2 nanoparticles mainly expose the less reactive {111} plane which lead to the CeO_2 nanoparticles shows a rather low catalytic activity relative to CeO_2 nanowires and nanorods [92]. Theoretical calculation also proved that the reactivity of CO oxidation on the CeO_2 surface planes follows the order of (100) > (110) > (111) [93–95].

What's more, recent application of CeO_2 for dephosphorylation reaction has also raise great concern, particularly in biological fields and waste treatment [96–100]. A case in point is that the decomposition of organophosphates. As vxshown in Fig. 8h, when Nitrophenyl disodium orthophosphate (p-NPP) was hydrolyzed to para-nitrophenol (p-NP) catalyzed by ceria, nano octahedron gives the highest yield of p-NP (89%) by 8 h followed by the nanorod (71%) and the nano cubic (9%). In addition, the different CeO_2 morphologies can show different catalytic performance when catalyze H_2O_2 reduction, and it can be evaluated in the presence of the dye molecule, tetramethylbenzidine (TMB). As shown in Fig. 8i, under certain reaction conditions, the presence of CeO_2 nano cubic can highly accelerate the conversion of H_2O_2, the nanorods and nano octahedron behave a little bit worse than nanocubes [101].

Except for pure CeO_2, various CeO_2-based hybrids own excellent catalytic performance as well. For instance, CeO_2 can exhibit high activity for CO removal by catalytic oxidation with high durability and shows attractive photodegradation properties as well. Also, it makes CeO_2 as a component of the modern automotive three-way catalysts to reduce the emission of gas engines [102]. Furthermore, it has been considered in fluid-cracking catalysts, oxidation catalysts and hydrocarbon reforming catalysts [103]. A summary of CO oxidation or photodegradation properties towards various CeO_2-based hybrids are shown in Tab. 5.
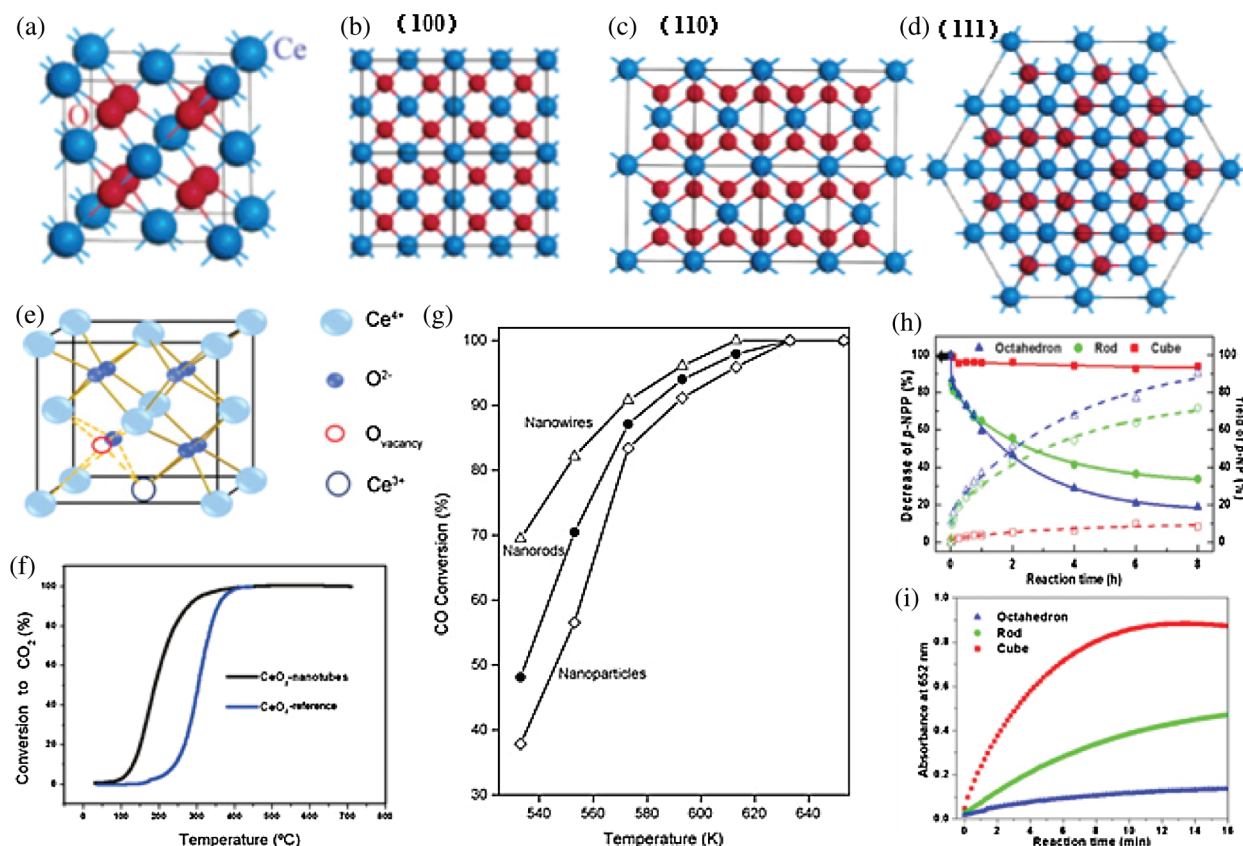
Figure 8: (a) Unit cell of the CeO_2 structure. (b–d) the (100) [or (200)], (110) and (111) plans of the CeO_2 structure. Adopted from Wang et al. [81], Copyright © 2003 American Chemical Society. (e) Schematic representation of CeO_2 cubic fluorite structure along with oxygen vacancy and Ce^{3+} in the lattice site. Adopted from Choudhury et al. [90], Copyright 2011 Elsevier B.V. (f) light-off curve corresponding to CeO_2 nanotubes and powder. Adopted from González-Rovira et al. [91], Copyright © 2009 American Chemical Society. (g) CO conversions over the CeO_2 nanomaterials. Adopted from Tana et al. [28], Copyright © 2009 Elsevier B.V. (h,i) Time-dependent activity of CeO_2 morphologies. Adopted from Tan et al. [101], Copyright © 2020 American Chemical Society

Table 5: Brief summary of catalytic efficiency of CeO_2 and various CeO_2-based hybrids

Catalysts	Specific application	Catalytic efficiency	Ref.
CeO_2(nanosphere)	CO conversion	100% at 380°C	[104]
CeO_2(sphere)	CO conversion	90% at 330°C	[26]
CeO_2(nanorods)	CO conversion	50% at 265°C	[25]
CeO_2(spindle-like)	CO conversion	50% at 250°C	[25]
CeO_2(nanoplates)	CO conversion	90% at 315°C	[105]
Ag/CeO_2	CO conversion	96.5% at 70°C	[26]

(Continued)

Table 5 (continued).

Catalysts	Specific application	Catalytic efficiency	Ref.
CdS/CeO_2	Degradation of Rhodamine B(RhB)	97% in 48 min	[106]
CeO_2/Ce_2O_3	Degradation of methylene bule (MB)	24 in 120 min	[107]
CeO_2/ZnO	Degradation of direct blue-15	95% in 120 min	[108]
$CeO_2/RGAs$	Degradation of RhB	85% in 120 min	[109]
CeO_2/Tb_2O_3	Degradation of MB	93% in 75 min	[110]
CeO_2/Co_3O_4	Degradation of MB/methyl red (MR)	99.65%/99.51% in 60 min	[111]
CeO_2/V_2O_5	Degradation of MB	64.2% in 210 min	[112]
CeO_2/CuO	Degradation of MB	70.1% in 210 min	[112]
$CeO_2/FACs$	Degradation of MB	60% in 300 min	[113]
$rGO-CeO_2$	Degradation of MB	72% in 50 min	[114]
CeO_2-SnO_2	Degradation of Direct Black 38	~60% in 240 min	[115]
$CeO_2/alumina$	Degradation of Congo red (CR)	90% in 120 min	[116]
$CeO_2/Nylon$	Degradation of MO	94.32% in 60 min	[117]

4.3 Application in Solid Oxide Fuel Cell Electrolyte Materials

Solid oxide fuel cells (SOFC) is attractive for its environmentally friendly properties. A solid oxide fuel cell is a structure of solid components that converts chemical energy into electrical energy. The core of a solid oxide fuel cell is an electrolyte made of ceramic materials that conduct by oxygen ions. Nano-ceria have unsurmountable advantages in fuel cells [118–121]. Meanwhile, nanometer CeO_2 can easily form high-density ceramic isolation layer after sheet pressing, sintering and other molding processes. The concentration of oxygen ion vacancy in nano-CeO_2 doped with bivalent or trivalent ions will be greatly increased, and higher ionic conductivity can be obtained at a relatively low operating temperature. Furthermore, the ceria-based anode was reported to be effective in preventing carbon formation and also to show good tolerance to sulfur [122,123]. Nanometer CeO_2-based electrolyte materials gradually replace the traditional ZrO_2-based electrolyte due to their excellent ionic conductivity and low activation energy.

Usually, CeO_2 is used in SOFC in three places: (1) doped-CeO_2 is used as an electrolyte in some designs. (2) CeO_2 is used as a barrier layer for cathodes to prevent reaction with the YSZ (yttria-stabilized zirconia) electrolyte, and (3) CeO_2 is sometimes added as a catalyst in both cathodes and anodes [124,125].

Li et al. [126] have proved that CeO_2 nanocubic used as electrolyte in SOFC can exhibit remarkable performance. The mechanism of the ionic transporting in CeO_2 nanocubes SOFCs are illustrated in Fig. 9a, and this design realized the higher power output with lower activation energy, at the same time, it owns good ionic conductivity. It is advisable to focus much eyesight on the morphology of catalyst during the electrode assembly stage. For instance, $Pd@CeO_2$ core-shell systems are found to be valid anodic catalysts with H_2 and CH_4 as fuels, and the core-shell structure can provide extra stabilization. The synthetic design included a salinization step of the YSZ so as to make a well-proportioned coverage of the electrode with the $Pd@CeO_2$ nanoparticles, as shown in Fig. 9b. The catalyst activities were maintained at high temperature during oxidative and operative reduction conditions [127]. Development of an anode material for a solid oxide fuel cell that is widely recognized to be an important technical objective.
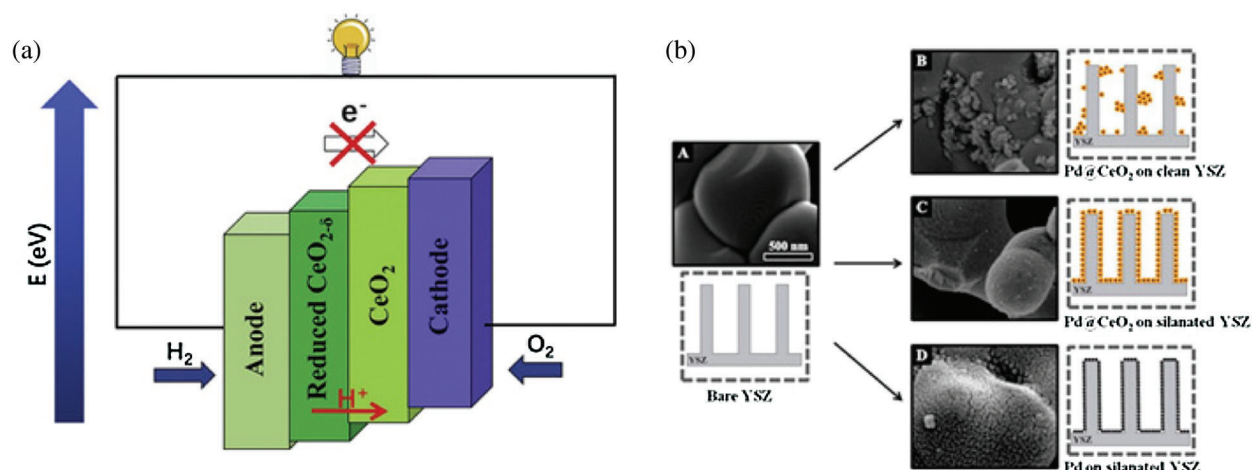
Figure 9: (a) The mechanism of the ionic transporting in CeO_2 nanocubes SOFCs. Adopted from Li et al. [126] Hydrogen Energy Publications LLC. Copyright 2018 Elsevier Ltd. (b) SEM images with schematic representations of (A) bare YSZ, (B) $Pd@CeO_2$ nanoparticles deposited on a clean YSZ porous electrode, (C) $Pd@CeO_2$ nanoparticles deposited on silanated YSZ porous electrode and (D) Uncoated Pd nanoparticles deposited on silanated YSZ porous electrode. YSZ (yttria-stabilized zirconia) Adopted from Adijanto et al. [127], Copyright 2013 American Chemical Society

4.4 Application in UV-Resistant Coatings

CeO_2 Oxides are potential materials for ultraviolet (UV) absorbent, because the absorption at 400 nm is the strongest for any oxide [128]. Usually, the mode that nanoparticles protect fibers from UV irradiation by absorbing UV. CeO_2 can strongly absorb ultraviolet light whose wavelength is less than 400 nm, so it is widely used in the field of ultraviolet shielding coating. Correspondingly, UV absorbance is becoming a significant indicator to evaluate the absorption properties of nanoparticles. As shown in Figs. 10a and 10b, the CeO_2 or CeO_2 heterostructure express strong absorption of ultraviolet [129,130]. The main factor of absorption of ultraviolet light by CeO_2 is the charge transfer between the internal O_2p state and Ce4f state [131]. CeO_2, owing to the quantum size effect of nanomaterials, compared with bulk materials (400 nm), ultraviolet absorption has a greater blue shift [132], so it has a broad potential application in the field of anti-ultraviolet coating.
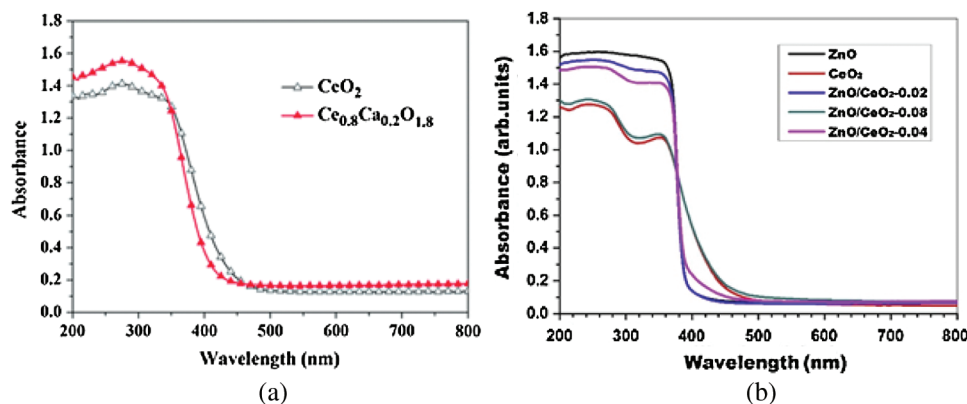
Figure 10: (a) UV-vis absorption spectra of CeO_2 and $Ce_{0.8}Ca_{0.2}O_{1.8}$. Adopted from Zhu et al. [129], Copyright 2014 The Royal Society of Chemistry. (b) UV-Vis absorption spectra of the ZnO/CeO_2 heterostructured nanocomposites with different atom molar ratios of Ce to Zn. Adopted from He et al. [130], Copyright © 2014 Elsevier B.V

4.5 Application in Chemical Mechanical Polishing

With the rapid development of optical technology and integrated circuit technology, the requirement for precision and ultra-precision polishing of optical components and chemical mechanical polishing technology of integrated circuits are increasingly high. CeO_2 polishing powder has many advantages, such as strong cutting ability, fast polishing rate, high smoothness, high levelling quality, good working conditions, small pollution, long service life, etc. therefore, it occupies an important and irreplaceable position in the fields of optical precision polishing and chemical mechanical polishing [133]. As the second-generation polishing fluid for grinding particles, CeO_2 overcomes the shortcomings of traditional silicon forming butterfly defect at the isolation of shallow grooves in large integrated circuits through the joint action of physical and chemical properties [134–136], thus it becomes one of the significant product types at present.

For instance, Deng et al. [137] use CeO_2 slurry to polish single-crystal SiC by electro-chemical mechanical polishing (ECMP). The experimental setup of ceria-slurry they used is shown in Fig. 11a. They compared three SiC substrates surface treated by different means. Fig. 11b shows SEM image of the diamond-abrasive polishing surface, on which many scratches can be observed. Fig. 11c shows the SEM image of the area outside the ECMP-processed area. The distinct anodic oxidation occurred on the surface due to the whole surface of the sample was immersed in CeO_2 slurry. Fig. 11d shows the SEM image of the ECMP-processed area. A smooth and scratch-free surface can be obtained. The results manifest that ceria-slurry-based ECMP is very effective for the flattening of SiC. In conclusion, CeO_2 play an important role in chemical mechanical polishing.
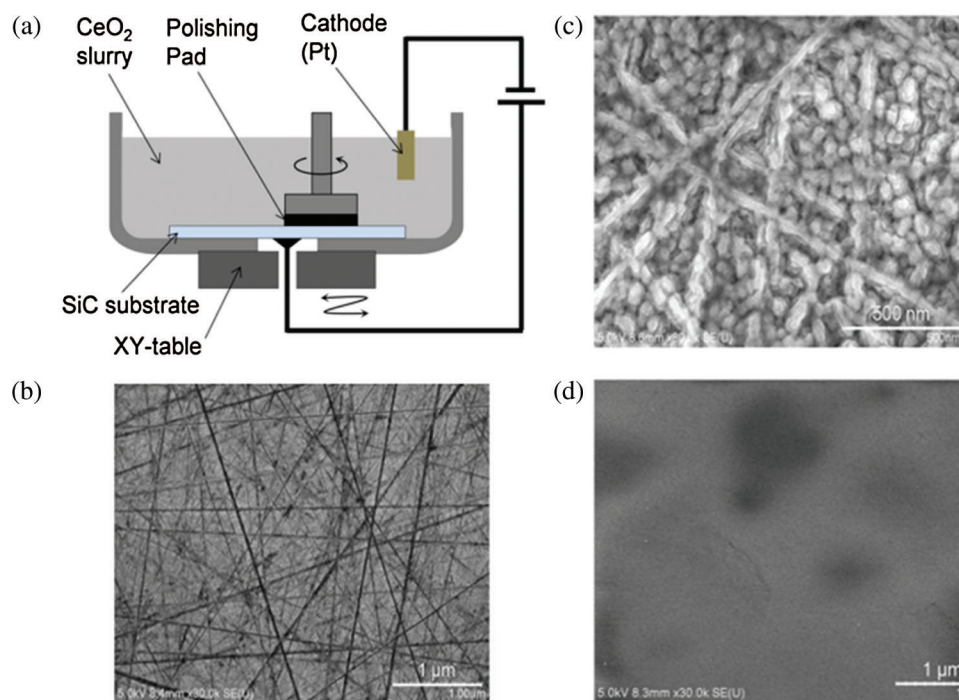
Figure 11: (a) Experimental setup of ceria-slurry-based ECMP. (b) SEM images of diamond-abrasive-polished SiC surfaces. (c) SEM images of anodically oxidized SiC surfaces. (d) SEM images of ECMP-processed SiC surface. Adopted from Deng et al. [137], Copyright 2015 Elsevier B.V

4.6 Other Applications

Except for the applications motioned above, the excellent properties also make the CeO_2 apply to many other fields. Such as sensor technologies [138,139], magnetic materials [140], optical materials [141], supercapacitors [142], water treatment and so on. To be specific, nano ceria also shows tremendous potentialities in biomedical application [143,144]. It is proved that nano-ceria could protect primary cells from the pernicious effects of radiation therapy [145] and to restrain retinal degeneration caused by intracellular peroxides [146]. What's more, nanoceria has been served as a novel therapy for chronic inflammation [147]. Some emerging application also plays an important role in ceria nanomaterials. It can be used to catalyze steam, dry and autothermal reforming of hydrocarbons or oxygenated compounds [148–150]. Oxidation of volatile organic compounds [151,152], dehalogenation [153,154] and so forth.

5 Summary and Outlook

This review highlights a series of CeO_2 micro/nanostructure with different morphologies and its main applications. we introduced the detailed synthesis process of each micro/nano morphology from different dimensionality, respectively. therein, it is much more difficult to control the crystal growth in two dimensions for its cubic crystal structure has no intrinsic driving force. Simultaneously, the main exposed crystalline planes of different morphologies are introduced as well. The main influencing factors of forming different morphologies were further discussed when synthesize CeO_2 micro/nanostructure via liquid-phase method. Interestingly, it is easy to find that the various micro/nano morphologies can be delicately controlled by changing the synthesis methods or adjusting the reaction parameters. Simultaneously, it is attractive that one morphology can convert into another by adjusting hydrothermal parameters. It is well known that functionality of CeO_2 nanomaterials, to a large extent, depends on the morphologies and size of the nanocrystals. Thus, it is significant to synthesis CeO_2 with controllable micro/nano morphologies. Correspondingly, it can be applied to corresponding fields according to its structure and properties.

Although plenty of attention has been paid to synthesis of ceria nanomaterials over the past few years, and future research is supposed to focus more on a better understanding of how synthetic techniques, composition, size, and morphology affect the properties of materials. It is attractive that theoretical calculation can provide a guidance on the rational design of highly reactive CeO_2-based catalysts. The valence and defect structure of CeO_2 was proved to play a significant part in its application. For example, by controlling the density and nature of the oxygen vacancies could tailor the reactivity of ceria-based catalysts. In this way, better activity and selectivity for a specific catalytic reaction can be realized when designing the catalysts, especially, for the metal-ceria interface. The reaction mechanism can be clarified by combination of first-principle calculation and new characterization approaches. Meanwhile, simulation prediction and first-principle calculation are useful in identification or design of appropriate CeO_2-based nanomaterials [155,156].

Hitherto, some encouraging result has been achieved, liquid-phase is a promising method for preparing nanostructure materials. Great challenge still exists to synthesize the small size and regular morphology nanostructure CeO_2 via solid-phase method. As for gas-phase method, the primary problem which need to be solved is to cut down the high price of the reaction equipment and make the reaction easy to operate. In addition, CeO_2 is considered an ideal candidate in superhydrophobic coatings for its large robust nature and high thermal stability. It has great potential application value in preservation industry. In the future, CeO_2-based nanomaterials will occupy an important position in energy conversion (fuel cell or the renewable production of fuels from solar energy), energy storage (lithium-air batteries), environment protection and so forth.

Conflicts of Interest: The authors declare that they have no conflicts to report regarding the present study.

References

1. Song, X. L., Wang, H. B., Wu, X. L., Qiu, G. Z. (2004). Preparation and applications of CeO_2 nanoparticles. *Chinese Rare Earths, 25(3),* 55–58 (in Chinese). DOI 10.1117/12.528072.

2. Yu, H., Bai, Y., Zong, X., Tang, F. Q., Lu, G. Q. et al. (2012). Cubic CeO_2 nanoparticles as mirror-like scattering layers for efficient light harvesting in dye-sensitized solar cells. *Chemical Communication, 48(59),* 7386–7388. DOI 10.1039/c2cc32239k.

3. Arul, N. S., Lee, Y. H., Lee, D. U., Kim, T. W., Nanosd, J. (2015). Enhancement of the power conversion efficiency in the inverted organic solar cells fabricated utilizing a CeO_2 interlayer between the poly (3-hexylthiophene) (P3HT): [6,6]-phenyl C_{61} butyric acid methyl ester and the cathode. *Journal of Nanoscience and Nanotechnology, 15(1),* 232–235. DOI 10.1166/jnn.2015.8401.

4. Sun, B., Han, P., Zhao, W. X., Liu, P. (2014). White-light-controlled magnetic and ferroelectric properties in multiferroic $BiFeO_3$ square nanosheets. *Journal of Physical Chemistry C, 118(32),* 18814–18819. DOI 10.1021/jp5064885.

5. Li, G., Wang, Q., Zhao, B., Zhou, R. (2012). A new insight into the role of transition metals doping with CeO_2-ZrO_2 and its application in Pd-only three-way catalysts for automotive emission control. *Fuel, 92(1),* 360–368. DOI 10.1016/j.fuel.2011.07.028.

6. Kempaiah, D. M., Yin, S., Sato, T. (2011). A facile and quick solvothermal synthesis of 3D microflower CeO_2 and Gd: CeO_2 under subcritical and supercritical conditions for catalytic applications. *CrystEngComm, 13(3),* 741–746. DOI 10.1039/C0CE00611D.

7. Dong, Y. C., Li, D. F., Hampshire, S., Zhou, J. E., Dickinson, C. et al. (2013). A high-strength Sm-doped CeO_2 oxide-ion conducting electrolyte membrane for solid oxide fuel cell application. *RSC Advances, 3(38),* 17395–17401. DOI 10.1039/c3ra42626b.

8. Huang, Y. H., Dass, R. I., Xing, Z. L., Goodenough, J. B. (2006). Double perovskites as anode materials for solid-oxide fuel cells. *Science, 312(5771),* 254–257. DOI 10.1126/science.1125877.

9. Rey-Garcia, F., Flores-Arias, M. T., Gomez-Reino, C., De La Fuente, G. F., Assenmacher, W. et al. (2012). Structural and optical characterization of ZrO_2: CeO_2 slab waveguides obtained via sol-gel. *Optical Materials, 35(2),* 97–101. DOI 10.1016/j.optmat.2012.07.016.

10. Feng, X. D., Sayle, D. C., Wang, Z. L., Paras, M. S., Santora, B. et al. (2006). Converting ceria polyhedral nanoparticles into single-crystal nanospheres. *Science, 312(5779),* 1504–1508. DOI 10.1126/science.1125767.

11. Abdel-Hameed, S. A. M., Margha, F. H., Ouis, M. A. (2013). Effect of CeO_2 on the crystallization behavior and magnetic properties of Zn-ferrite glass ceramics. *Journal of Alloys and Compounds, 554,* 371–377. DOI 10.1016/j.jallcom.2012.11.132.

12. Gong, J. F., Meng, F. M., Yang, X., Fan, Z. H., Li, H. J. (2016). Controlled hydrothermal synthesis of triangular CeO_2 nanosheets and their formation mechanism and optical properties. *Journal of Alloys and Compounds, 689,* 606–616. DOI 10.1016/j.jallcom.2016.08.030.

13. Wu, G. L., Cheng, Y. H., Feng, X., Jia, Z. R., Qian, X. et al. (2016). Morphology-controlled synthesis, characterization and microwave absorption properties of nanostructured 3D CeO_2. *Materials Science in Semiconductor Processing, 41,* 6–11. DOI 10.1016/j.mssp.2015.06.077.

14. Wei, Y., Zhao, Z., Liu, J., Xu, C., Jiang, G. et al. (2013). Design and synthesis of 3D ordered macroporous CeO_2-supported pt@ CeO_2-δ core-shell nanoparticle materials for enhanced catalytic activity of soot oxidation. *Small, 9 (23),* 3957–3963. DOI 10.1002/smll.201301027.

15. Liu, Z. Q., Na, L. N., Zhao, H. Y., Zhang, Y., Huang, Y. H. et al. (2017). Regulating the active species of $Ni(OH)_2$ using CeO_2: 3D CeO_2/$Ni(OH)_2$/carbon foam as an efficient electrode for the oxygen evolution reaction. *Chemical Science, 8,* 3211–3217.

16. Wu, Q., Zhang, F., Xiao, P., Tao, H. S., Wang, X. Z. et al. (2008). Great influence of anions for controllable synthesis of CeO_2 nanostructures: from nanorods to nanocubes. *Journal of Physical Chemistry C, 112(44),* 17076–17080. DOI 10.1021/jp804140e.

17. Chen, G. Z., Sun, S. X., Sun, X., Fan, W. L., You, T. (2009). Formation of CeO_2 nanotubes from $Ce(OH)CO_3$ nanorods through Kirkendall diffusion. *Inorganic Chemistry, 48(4),* 1334–1338. DOI 10.1021/ic801714z.

18. González-Rovira, L., Sánchez-Amaya, J. M., López-Haro, M., del Rio, E., Hungría, A. B. et al. (2009). Single-step process to prepare CeO_2 nanotubes with improved catalytic activity. *Nano Letters, 9(4),* 1395–1400. DOI 10.1021/nl803047b.

19. Zhou, H. P., Zhang, Y. W., Si, R., Zhang, L. S., Song, W. G. et al. (2008). Dimension-manipulated ceria nanostructures (0D uniform nanocrystals, 2D polycrystalline assembly, and 3D mesoporous framework) from cerium octylate precursor in solution phases and their CO oxidation activities. *Journal of Physical Chemistry C, 112(51),* 20366–20374. DOI 10.1021/jp807091n.

20. Carey, G. H., Abdelhady, A. L., Ning, Z., Thon, S. M., Bakr, O. M. et al. (2015). Colloidal quantum dot solar cells. *Chemical Reviews, 115(23),* 12732–12763. DOI 10.1021/acs.chemrev.5b00063.

21. Ye, M. Y., Zhao, Z. H., Hu, Z. F., Liu, L. Q., Ji, H. M. et al. (2017). 0D/2D heterojunctions of vanadate quantum dots/graphitic carbon nitride nanosheets for enhanced visible-light-driven photocatalysis. *Angewandate Chemie International Edition, 56(29),* 8407–8411. DOI 10.1002/anie.201611127.

22. Zhou, K., Wang, X., Sun, X., Peng, Q., Li, Y. (2005). Enhanced catalytic activity of ceria nanorods from well-defined reactive crystal planes. *Journal of Catalysis, 229(1),* 206–212. DOI 10.1016/j.jcat.2004.11.004.

23. Mai, H. X., Sun, L. D., Zhang, Y. W., Si, R., Feng, W. et al. (2005). Shape-selective synthesis and oxygen storage behavior of ceria nanopolyhedra, nanorods, and nanocubes. *Journal of Physical Chemistry B, 109(51),* 24380–24385. DOI 10.1021/jp055584b.

24. Imagawa, H., Suda, A., Yamamura, K., Sun, S. (2016). Monodisperse CeO_2 nanoparticles and their oxygen storage and release properties. *Journal of Physical Chemistry C, 115(5),* 1740–1745. DOI 10.1021/jp109878j.

25. Ho, C., Yu, J. C., Kwong, T., Mak, A. C., Lai, S. (2005). Morphology-controllable synthesis of mesoporous CeO_2 nano- and microstructures. *Chemistry of Materials, 17(17),* 4514–4522. DOI 10.1021/cm0507967.

26. Liang, X., Xiao, J., Chen, B., Li, Y. (2010). Catalytically stable and active CeO_2 mesoporous spheres. *Inorganic Chemistry, 49(18),* 8188–8190. DOI 10.1021/ic100795p.

27. Cai, W., Zhang, B., Li, Y., Xu, Y., Shen, W. (2007). Hydrogen production by oxidative steam reforming of ethanol over an Ir/CeO_2 catalyst. *Catalysis Communications, 8(11),* 1588–1594. DOI 10.1016/j.catcom.2007.01.017.

28. Tana, Zhang, M., Li, J., Li, H., Li, Y., Shen, W. (2009). Morphology-dependent redox and catalytic properties of CeO_2 nanostructures: nanowires, nanorods and nanoparticles. *Catalysis Today, 148(1–2),* 179–183. DOI 10.1016/j.cattod.2009.02.016.

29. Yadav, T. P., Srivastava, O. N. (2012). Synthesis of nanocrystalline cerium oxide by high energy ball milling. *Ceramics International, 38(7),* 5783–5789. DOI 10.1016/j.ceramint.2012.04.025.

30. Shukla, N., Liu, C., Jones, P. M., Weller, D. (2003). FTIR study of surfactant bonding to FePt nanoparticles. *Journal of Magnetism and Magnetic Materials, 266(1–2),* 178–184. DOI 10.1016/S0304-8853(03)00469-4.

31. Sun, S. (2006). Recent advances in chemical synthesis, self-assembly, and applications of FePt nanoparticles. *Advanced Materials, 18(4),* 393–403. DOI 10.1002/adma.200501464.

32. Hailstone, R. K., Difrancesco, A. G., Leong, J. G., Allston, T. D., Reed, K. J. (2009). A study of lattice expansion in CeO_2 nanoparticles by transmission electron microscopy. *Journal of Physical Chemistry C, 113(34),* 15155–15159. DOI 10.1021/jp903468m.

33. Jing, O. Y., Yang, H. M. (2009). Investigation of the oxygen exchange property and oxygen storage capacity of cexZr1-xO$_2$ nanocrystals. *Journal of Physical Chemistry C, 113(31),* 6921–6928. DOI 10.1021/jp902080p.

34. Hirano, M., Suda, A. (2010). Oxygen storage capacity, specific surface area, and pore-size distribution of ceria-zirconia solid solutions directly formed by thermal hydrolysis. *Journal of the American Ceramic Society, 86(12),* 2209–2211. DOI 10.1111/j.1151-2916.2003.tb03634.x.

35. Ke, J., Xiao, J., Zhu, W., Liu, H., Si, R. et al. (2013). Dopant-induced modification of active site structure and surface bonding mode for high-performance nanocatalysts: CO oxidation on capping-free (110)-oriented CeO_2:

Ln (Ln = La – Lu) nanowires. *Journal of the American Chemical Society, 135(40),* 15191–15200. DOI 10.1021/ja407616p.

36. Wu, Q., Zhang, F., Xiao, P., Tao, H., Wang, X. et al. (2008). Great influence of anions for controllable synthesis of CeO_2 nanostructures: from nanorods to nanocubes. *Journal of Physical Chemistry C, 112(44),* 17076–17080. DOI 10.1021/jp804140e.

37. Yu, R., Yan, L., Zheng, P., Chen, J., Xing, X. (2008). Controlled synthesis of CeO_2 flower-like and well-aligned nanorod hierarchical. *Journal of Physical Chemistry C, 112(50),* 19896–19900. DOI 10.1021/jp806092q.

38. Li, X. P., Sun, Y. L., Xu, Y. Y., Chao, Z. S. (2018). UV-resistant and thermally stable superhydrophobic CeO_2 nanotubes with high water adhesion. *Small, 14(27),* 1801040–1801051. DOI 10.1002/smll.201801040.

39. Tang, Z., Zhang, Y., Xu, Y. (2011). A facile and high-yield approach to synthesize one-dimensional CeO_2 nanotubes with well-shaped hollow interior as a photocatalyst for degradation of toxic pollutants. *RSC Advances, 1(9),* 1772–1777. DOI 10.1039/c1ra00518a.

40. Chen, G., Xu, C., Song, X., Zhao, W., Ding, Y. et al. (2008). Interface reaction route to two different kinds of CeO_2 nanotubes. *Inorganic Chemistry, 47(2),* 723–728. DOI 10.1021/ic701867f.

41. Li, H., Meng, F., Gong, J., Fan, Z., Qin, R. (2017). Structural, morphological and optical properties of shuttle-like CeO_2 synthesized by a facile hydrothermal method. *Journal of Alloys and Compounds, 722,* 489–498. DOI 10.1016/j.jallcom.2017.06.156.

42. He, H., Yang, P., Li, J., Shi, R., Chen, L. (2016). Controllable synthesis, characterization, and CO oxidation activity of CeO_2 nanostructures with various morphologies. *Ceramics International, 42(6),* 7810–7818. DOI 10.1016/j.ceramint.2016.02.005.

43. La, R., Hua, Z., Li, H., Shang, X., Yang, Y. (2004). Template synthesis of CeO_2 ordered nanowire arrays. *Materials Science and Engineering A, 368(1–2),* 145–148. DOI 10.1016/j.msea.2003.10.279.

44. González-Rovira, L., Sánchez-Amaya, J́. M., López-Haro, M., del Rio, E., Hungría, A. B. et al. (2009). Single-step process to prepare CeO_2 nanotubes with improved catalytic activity. *Nano Letters, 9(4),* 1395–1400. DOI 10.1021/nl803047b.

45. Liu, B., Li, Q. J., Du, X. B., Liu, B., Yao, M. G. et al. (2011). Facile hydrothermal synthesis of CeO_2 nanosheets with high reactive exposure surface. *Journal of Alloys and Compounds, 509(23),* 6720–6724. DOI 10.1016/j.jallcom.2011.03.156.

46. Lin, H. L., Wu, C. Y., Chiang, R. K. (2010). Facile synthesis of CeO_2 nanoplates and nanorods by [1 0 0] oriented growth. *Journal of Colloid and Interface Science, 341(1),* 12–17. DOI 10.1016/j.jcis.2009.04.047.

47. Yu, T., Lim, B., Xia, Y. N. (2010). Aqueous-phase synthesis of single-crystal ceria nanosheets. *Angewandate Chemie International Edition, 49(26),* 4484–4487. DOI 10.1002/anie.201001521.

48. Wang, D. Y., Kang, Y. J., Doan-Nguyen, V., Chen, J., Küngas, R. et al. (2011). Synthesis and oxygen storage capacity of two-dimensional ceria nanocrystals. *Angewandate Chemie International Edition, 50(19),* 4378–4381. DOI 10.1002/anie.201101043.

49. Imagawa, H., Sun, S. H. (2012). Controlled synthesis of monodisperse CeO_2 nanoplates developed from assembled nanoparticles. *Journal of Physical Chemistry C, 116(4),* 2761–2765. DOI 10.1021/jp210324x.

50. Pan, C., Zhang, D., Shi, L. (2008). CTAB assisted hydrothermal synthesis, controlled conversion and CO oxidation properties of CeO_2 nanoplates, nanotubes, and nanorods. *Journal of Solid State Chemistry, 181(6),* 1298–1306. DOI 10.1016/j.jssc.2008.02.011.

51. Gong, J., Meng, F., Yang, X., Fan, Z., Li, H. (2016). Controlled hydrothermal synthesis of triangular CeO_2 nanosheets and their formation mechanism and optical properties. *Journal of Alloys and Compounds, 689,* 606–616. DOI 10.1016/j.jallcom.2016.08.030.

52. Zhou, K., Wang, X., Sun, X., Peng, Q., Li, Y. (2005). Enhanced catalytic activity of ceria nanorods from well-defined reactive crystal planes. *Journal of Catalysis, 229(1),* 206–212. DOI 10.1016/j.jcat.2004.11.004.

53. Guo, Y., Fang, Z., Xu, X. (2006). An analytic solution of a linear camera self-calibration. In *The Sixth World Congress on Intelligent Control and Automation, WCICA,* pp. 9930–9934.

54. Service, R. F. (2005). How far can we push chemical self-assembly? *Science, 309(5731),* 95. DOI 10.1126/science.309.5731.95.

55. Whitesides, G. M., Boncheva, M. (2002). Beyond molecules: self-assembly of mesoscopic and macroscopic components. *Proceedings of the National Academy of Sciences of the United States of America, 99(8),* 4769–4774. DOI 10.1073/pnas.082065899.

56. Hu, J., Chen, W., Zhao, X., Su, H., Chen, Z. (2018). Anisotropic electronic characteristics, adsorption, and stability of low-index $BiVO_4$ surfaces for photoelectrochemical applications. *ACS Applied Materials & Interfaces, 10(6),* 5475–5484. DOI 10.1021/acsami.7b15243.

57. Lee, M., Delgado, A. (2017). *A Raman study of CeO_2 nanomaterials with different morphologies (Master Thesis).* Department of Chemical and Biological Engineering Friedrich-Alexander University Erlangen-Nürnberg, Erlangen, pp. 9–20.

58. Yan, L., Yu, R., Chen, J., Xing, X. (2008). Template-free hydrothermal synthesis of CeO_2 nano-octahedrons and nanorods: investigation of the morphology evolution. *Crystal Growth & Design, 8(5),* 1474–1477. DOI 10.1021/cg800117v.

59. Zhong, L., Hu, J., Cao, A., Liu, Q., Song, W. et al. (2007). 3D flowerlike ceria micro/nanocomposite structure and its application for water treatment and CO removal. *Chemistry of Materials, 19(7),* 1648–1655. DOI 10.1021/cm062471b.

60. Matinise, N., Fuku, X. G., Kaviyarasu, K., Mayedwa, N., Maaza, M. (2017). ZnO nanoparticles via *Moringa oleifera* green synthesis: physical properties & mechanism of formation. *Applied Surface Science, 406,* 339–347. DOI 10.1016/j.apsusc.2017.01.219.

61. Kaviyarasu, K., Manikandan, E., Kennedy, J., Maaza, M. (2016). Synthesis and analytica applications of photoluminescent carbon nanosheet by exfoliation of graphite oxide without purification. *Journal of Materials Science: Materials in Electronics, 27(12),* 13080–13085. DOI 10.1007/s10854-016-5451-z.

62. Pan, C., Hang, D., Shi, L., Fang, J. (2008). Template-free synthesis, controlled conversion, and CO oxidation properties of CeO_2 nanorods, nanotubes, nanowires, and nanocubes. *European Journal of Inorganic Chemistry, 2008(15),* 2429–2436. DOI 10.1002/ejic.200800047.

63. Xi, G. C., Xiong, K., Zhao, Q. B., Zhang, R., Zhang, H. B. et al. (2006). Nucleation-dissolution-recrystallization: a new growth mechanism for t-selenium nanotubes. *Crystal Growth & Design, 6(2),* 577–582. DOI 10.1021/cg050444c.

64. Lu, J., Xie, Y., Xu, F., Zhu, L. Y. (2002). Study of the dissolution behavior of selenium and tellurium in different solvents—a novel route to Se, Te tubular bulk single crystals. *Journal of Materials Chemistry, 12(9),* 2755–2761. DOI 10.1039/B204092A.

65. Sun, C. W., Li, H., Chen, L. Q. (2012). Nanostructured ceria-based materials: synthesis, properties, and applications. *Energy & Environmental Science, 5(9),* 8475–8505. DOI 10.1039/c2ee22310d.

66. Agarwal, S., Lefferts, L., Mojet, B. L., Ligthart, D. A. J. M., Hensen, E. J. M. et al. (2013). Exposed surfaces on shape-controlled ceria nanoparticles revealed through AC-TEM and water-gas shift reactivity. *ChemSusChem, 6 (10),* 1898–1906. DOI 10.1002/cssc.201300651.

67. Zheng, S., Cheng, L., Fu, Q., Xiang, T., Hu, W. et al. (2016). Fabrication of micro-nanostructured superhydrophobic aluminum surface with excellent corrosion resistance and anti-icing performance. *RSC Advances, 6(83),* 79389–79400. DOI 10.1039/C6RA13447E.

68. He, C., Huang, J., Li, S., Meng, K., Zhang, L. et al. (2018). Mechanically resistant and sustainable cellulose-based composite aerogels with excellent flame retardant, sound-absorption and super-antiwetting ability for advanced engineering materials. *ACS Sustainable Chemistry & Engineering, 6(1),* 927–936. DOI 10.1021/acssuschemeng.7b03281.

69. Zheng, S., Li, C., Fu, Q., Li, M., Hu, W. et al. (2015). Fabrication of self cleaning superhydrophobic surface on aluminum alloys with excellent corrosion resistance. *Surface & Coatings Technology, 276,* 341–348. DOI 10.1016/j.surfcoat.2015.07.002.

70. Li, L., Huang, T., Lei, J., He, J., Qu, L. et al. (2015). Robust biomimetic-structural superhydrophobic surface on aluminum alloy. *ACS Applied Materials & Interfaces, 7(3),* 1449–1457. DOI 10.1021/am505582j.

71. Liu, Y., Wang, Q., Zhu, X., Yang, F., Akram, M. Y. et al. (2017). Preparation of superhydrophobic surface via one-step photopolymerization. *Materials Letters, 190,* 48–51. DOI 10.1016/j.matlet.2016.12.093.

72. Xiang, T., Zhang, M., Li, C., Zheng, S., Ding, S. et al. (2017). A facile method for fabrication of superhydrophobic surface with controllable water adhesion and its applications. *Journal of Alloys and Compounds, 704,* 170–179. DOI 10.1016/j.jallcom.2017.01.277.

73. Liu, Q., Chen, D., Kang, Z. (2015). One-step electrodeposition process to fabricate corrosion-resistant superhydrophobic surface on magnesium alloy. *ACS Applied Materials & Interfaces, 7(3),* 1859–1867. DOI 10.1021/am507586u.

74. Shen, Y., Tao, H., Chen, S., Xie, Y., Zhou, T. et al. (2014). Water repellency of hierarchical superhydrophobic Ti6Al4V surfaces improved by secondary nanostructures. *Applied Surface Science, 321,* 469–474. DOI 10.1016/j.apsusc.2014.10.044.

75. Ishizaki, T., Masuda, Y., Sakamoto, M. (2011). Corrosion resistance and durability of superhydrophobic surface formed on magnesium alloy coated with nanostructured cerium oxide film and fluoroalkylsilane molecules in corrosive NaCl aqueous solution. *Langmuir, 27(8),* 4780–4788. DOI 10.1021/la2002783.

76. Spezzati, G., Benavidez, A., Delariva, A. T., Su, Y., Hofmann, J. P. et al. (2019). Co oxidation by pd supported on CeO_2 (100) and CeO_2 (111) facets. *Applied Catalysis B: Environmental, 243,* 36–46. DOI 10.1016/j. apcatb.2018.10.015.

77. Wang, Z., Huang, Z., Brosnahan, J. T., Zhang, S., Guo, Y. et al. (2019). Ru/CeO_2 catalyst with optimized CeO_2 support morphology and surface facets for propane combustion. *Environmental Science & Technology, 53(9),* 5349–5358. DOI 10.1021/acs.est.9b01929.

78. Tao, Z., Chang, H. Z., Li, K. Z., Peng, Y., Li, X. et al. (2018). Different exposed facets VOx/CeO_2 catalysts for the selective catalytic reduction of no with NH_3. *Chemical Engineering Journal, 349,* 184–191. DOI 10.1016/j. cej.2018.05.049.

79. Afzal, S., Quan, X., Sen, L. (2019). Catalytic performance and an insight into the mechanism of CeO_2 nanocrystals with different exposed facets in catalytic ozonation of p-nitrophenol. *Applied Catalysis B: Environmental, 248,* 526–537. DOI 10.1016/j.apcatb.2019.02.010.

80. Wang, F., Li, C., Zhang, X., Wei, M., Evans, D. G. et al. (2015). Catalytic behavior of supported Ru nanoparticles on the {1 0 0} {1 1 0}, {1 1 1} facet of CeO_2. *Journal of Catalysis, 329,* 177–186. DOI 10.1016/j.jcat.2015.05.014.

81. Wang, Z. L., Feng, X. (2003). Polyhedral shapes of CeO_2 nanoparticles. *Journal of Physical Chemistry B, 107(49),* 13563–13566. DOI 10.1021/jp036815m.

82. Conesa, J. C. (1995). Computer modeling of surfaces and defects on cerium dioxide. *Surface Science, 339(3),* 337–352. DOI 10.1016/0039-6028(95)00595-1.

83. Branda, M. M., Ferullo, R. M., Causà, M., Illas, F. (2011). Relative stabilities of low index and stepped CeO_2 surfaces from hybrid and GGA + U implementations of density functional theory. *Journal of Physical Chemistry C, 115(9),* 3716–3721. DOI 10.1021/jp111427j.

84. Cao, X., Zhao, X., Hu, J., Chen, Z. (2020). First-principles investigation of electronic properties of bi2o4 (101)/bivo4 (010) heterojunction towards more efficient solar water splitting. *Physical Chemistry Chemical Physics, 22,* 2449–2456.

85. Campbell, C. T., Peden, C. H. F. (2005). Chemistry—oxygen vacancies and catalysis on ceria surfaces. *Science, 309(5735),* 713–714. DOI 10.1126/science.1113955.

86. Chueh, W. C., Falter, C., Abbott, M., Scipio, D., Furler, P. et al. (2010). High-flux solar-driven thermochemical dissociation of CO_2 and H_2O using nonstoichiometric ceria. *Science, 330(6012),* 1797–1801. DOI 10.1126/science.1197834.

87. Yang, L., Kresnawahjuesa, O., Gorte, R. J. (2001). A calorimetric study of oxygen-storage in pd/ceria and pd/ceria-zirconia catalysts. *Catalysis Letters, 72(1–2),* 33–37. DOI 10.1023/A:1009012610200.

88. Gorte, R. J., Zhao, S. (2005). Studies of the water-gas-shift reaction with ceria-supported precious metals. *Catalysis Today, 104(1),* 18–24. DOI 10.1016/j.cattod.2005.03.034.

89. Zhang, F., Wang, P., Koberstein, J., Khalid, S., Chan, S. (2004). Cerium oxidation state in ceria nanoparticles studied with X-ray photoelectron spectroscopy and absorption near edge spectroscopy. *Surface Science, 563(1–3),* 74–82. DOI 10.1016/j.susc.2004.05.138.

90. Choudhury, B., Choudhury, A. (2012). Ce^{3+} and oxygen vacancy mediated tuning of structural and optical properties of CeO_2 nanoparticles. *Materials Chemistry and Physics, 131(3),* 666–671. DOI 10.1016/j. matchemphys.2011.10.032.

91. González-Rovira, L., Sánchez-Amaya, J. M., López-Haro, M., Rio, E. D., Botana, F. J. (2009). Single-step process to prepare CeO_2 nanotubes with improved catalytic activity. *Nano Letters, 9(6),* 2511. DOI 10.1021/nl901292s.

92. Zhou, K., Wang, X., Sun, X., Peng, Q., Li, Y. (2005). Enhanced catalytic activity of ceria nanorods from well-defined reactive crystal planes. *Journal of Catalysis, 229(1),* 206–212. DOI 10.1016/j.jcat.2004.11.004.

93. Sayle, T. X. T., Parker, S. C., Catlow, C. R. A. (1994). The role of oxygen vacancies on ceria surfaces in the oxidation of carbon monoxide. *Surface Science, 316(3),* 329–336. DOI 10.1016/0039-6028(94)91225-4.

94. Sayle, D. C., Maicaneanu, S. A., Watson, G. W. (2002). Atomistic models for CeO_2 (111), (110), and (100) nanoparticles, supported on yttrium-stabilized zirconia. *Journal of the American Chemical Society, 124(38),* 11429–11439. DOI 10.1021/ja020657f.

95. Yang, Z., Woo, T. K., Baudin, M., Hermansson, K. (2004). Atomic and electronic structure of unreduced and reduced CeO_2 surfaces: a first-principles study. *Journal of Chemical Physics, 120(16),* 7741–7749. DOI 10.1063/1.1688316.

96. Xu, C., Qu, X. (2014). Cerium oxide nanoparticle: a remarkably versatile rare earth nanomaterial for biological applications. *NPG Asia Materials, 6(3),* e90. DOI 10.1038/am.2013.88.

97. Wang, H., Wan, K., Shi, X. (2018). Recent advances in nanozyme research. *Advanced Materials, 31(45),* 1805368. DOI 10.1002/adma.201805368.

98. Wang, Z. G., Bi, W. Z., Ma, S. C., Lv, N., Zhang, J. L. (2015). Facet-dependent effect of well-defined CeO_2 nanocrystals on the adsorption and dephosphorylation of phosphorylated molecules. *Particle & Particle Systems Characterization, 32(6),* 652–660. DOI 10.1002/ppsc.201400230.

99. Manto, M. J., Xie, P., Wang, C. (2017). Catalytic dephosphorylation using ceria nanocrystals. *ACS Catalysis, 7 (3),* 1931–1938. DOI 10.1021/acscatal.6b03472.

100. Yao, T., Tian, Z., Zhang, Y., Qu, Y. (2018). Phosphatase-like activity of porous nanorods of CeO_2 for the highly stabilized dephosphorylation under interferences. *ACS Applied Materials & Interfaces, 11(1),* 195–201. DOI 10.1021/acsami.8b17086.

101. Tan, Z., Li, G., Chou, H., Li, Y., Yi, X. et al. (2020). Differentiating surface Ce species among CeO_2 facets by solid-state NMR for catalytic correlation. *ACS Catalysis, 10(7),* 4003–4011. DOI 10.1021/acscatal.0c00014.

102. Kaspar, J., Fornasiero, P., Graziani, M. (1999). Use of CeO_2-based oxides in the three-way catalysts. *Catalysis Today, 50,* 285–298.

103. Sun, C. W., Li, H., Chen, L. Q. (2012). Nanostructured ceria-based materials: synthesis, properties, and applications. *Energy & Environmental Science, 5(9),* 8475–8505. DOI 10.1039/c2ee22310d.

104. Ta, N., Zhang, M., Li, J., Li, Y., Shen, W. (2008). Facile synthesis of CeO_2 nanospheres. *Chinese Journal of Catalysis, 29(11),* 1070–1072. DOI 10.1016/S1872-2067(09)60002-4.

105. Cui, R., Lu, W., Zhang, L., Yue, B., Shen, S. (2011). Template-free synthesis and self-assembly of CeO_2 nanospheres fabricated with foursquare nanoflakes. *Journal of Physical Chemistry C, 113(52),* 21520–21525. DOI 10.1021/jp9065168.

106. Gu, S., Chen, Y., Yuan, X., Wang, H., Zeng, G. (2015). Facile synthesis of CeO_2 nanoparticle sensitized CdS nanorod photocatalyst with improved visible-light photocatalytic degradation of rhodamine B. *RSC Advances, 5(97),* 79556–79564. DOI 10.1039/C5RA16114B.

107. Ma, R., Islam, M. J., Reddy, D. A., Kim, T. K. (2016). Transformation of CeO_2 into a mixed phase CeO_2/Ce_2O_3 nanohybrid by liquid phase pulsed laser ablation for enhanced photocatalytic activity through Z-scheme pattern. *Ceramics International, 42(16),* 18495–18502. DOI 10.1016/j.ceramint.2016.08.186.

108. Lamba, R., Umar, A., Mehta, S. K., Kansal, S. K. (2015). CeO_2-ZnO hexagonal nanodisks: efficient material for the degradation of direct blue 15 dye and its simulated dye bath effluent under solar light. *Journal of Alloy and Compounds, 620,* 67–73. DOI 10.1016/j.jallcom.2014.09.101.

109. Choi, J., Reddy, D. A., Islam, M. J., Ma, R., Kim, T. K. (2016). Self-assembly of CeO$_2$ nanostructures/reduced graphene oxide composite aerogels for efficient photocatalytic degradation of organic pollutants in water. *Journal of Alloys and Compounds, 688,* 527–536. DOI 10.1016/j.jallcom.2016.07.236.

110. Arul, N. S., Mangalaraj, D., Kim, T. W. (2015). Photocatalytic degradation mechanisms of CeO$_2$/Tb$_2$O$_3$ nanotubes. *Applied Surface Science, 349,* 459–464. DOI 10.1016/j.apsusc.2015.04.206.

111. Tang, Y., Zhang, M., Wu, Z., Chen, Z., Liu, C. et al. (2018). Synthesis and photocatalytic activity of p-n junction CeO$_2$/CO$_3$O$_4$ photocatalyst for the removal of various dyes from wastewater. *Materials Research Express, 5(4),* 045045. DOI 10.1088/2053-1591/aabdd8.

112. Saravanan, R., Joicy, S., Gupta, V. K., Narayanan, V., Stephen, A. (2013). Visible light induced degradation of methylene blue using CeO$_2$/V$_2$O$_5$ and CeO$_2$/CuO catalysts. *Materials Science and Engineering C, 33(8),* 4725–4731. DOI 10.1016/j.msec.2013.07.034.

113. Zhang, J., Wang, B., Li, C., Cui, H., Zhai, J. et al. (2014). Synthesis of novel CeO$_2$-BiVO$_4$/FAC composites with enhanced visible-light photocatalytic properties. *Journal of Environmental Sciences, 26(9),* 1936–1942. DOI 10.1016/j.jes.2014.07.006.

114. Kumar, S., Kumar, A. (2017). Enhanced photocatalytic activity of rGO-CeO$_2$ nanocomposites driven by sunlight. *Materials Science and Engineering B, 223,* 98–108. DOI 10.1016/j.mseb.2017.06.006.

115. Foletto, E. L., Battiston, S., Collazzo, G. C., Bassaco, M. M., Mazutti, M. A. (2012). Degradation of leather dye using CeO$_2$-SNO$_2$ nanocomposite as photocatalyst under sunlight. *Water Air & Soil Pollution, 223(9),* 5773–5779. DOI 10.1007/s11270-012-1313-3.

116. Latha, P., Prakash, K., Karuthapandian, S. (2017). Enhanced visible light photocatalytic activity of CeO$_2$/alumina nanocomposite: synthesized via facile mixing-calcination method for dye degradation. *Advanced Powder Technology, 28(11),* 2903–2913. DOI 10.1016/j.apt.2017.08.017.

117. Latha, P., Dhanabackialakshmi, R., Kumar, P. S., Karuthapandian, S. (2016). Synergistic effects of trouble free and 100% recoverable CeO$_2$/Nylon nanocomposite thin film for the photocatalytic degradation of organic contaminants. *Separation and Purification Technology, 168,* 124–133. DOI 10.1016/j.seppur.2016.05.038.

118. Qiao, Z., Xia, C., Cai, Y., Afzal, M., Wang, H. et al. (2018). Electrochemical and electrical properties of doped CeO$_2$-ZnO composite for low-temperature solid oxide fuel cell applications. *Journal of Power Sources, 392,* 33–40. DOI 10.1016/j.jpowsour.2018.04.096.

119. Wang, B., Zhu, B., Yun, S., Zhang, W., Wang, H. (2019). Fast ionic conduction in semiconductor CeO$_2$-δ electrolyte fuel cells. *NPG Asia Materials, 11(1),* 51. DOI 10.1038/s41427-019-0152-8.

120. Bhabu, K. A., Theerthagiri, J., Madhavan, J., Balu, T., Muralidharan, G. et al. (2016). Cubic fluorite phase of samarium doped cerium oxide (CeO$_2$)0.96Sm0.04 for solid oxide fuel cell electrolyte. *Journal of Materials Science: Materials in Electronics, 27(2),* 1566–1573. DOI 10.1007/s10854-015-3925-z.

121. Nurhasanah, I., Abdullah, M., Khairurrijal, K. (2008). Structure and morphology of neodymium-doped cerium oxide solid solution prepared by a combined simple polymer heating and D.C.-magnetron sputtering method. *AIP Conference Proceedings, 989,* 147–150.

122. Barnett, S. A. (2003). *Handbook of fuel cell technology.* Hoboken, NJ: Wiley.

123. He, H. P., Gorte, R. J., Vohs, J. M. (2005). Highly sulfur tolerant Cu-ceria anodes for SOFCs. *Electrochemical and Solid-State Letters, 8(6),* A279. DOI 10.1149/1.1896469.

124. Hladik, J. (1972). *Physics of electrolytes.* London: Academic Press.

125. Mogensen, M. (1994). Physical properties of mixed conductor solid oxide fuel cell anodes of doped CeO$_2$. *Journal of the Electrochemical Society, 141(8),* 2122–2128. DOI 10.1149/1.2055072.

126. Li, L., Zhu, B., Zhang, J., Yan, C., Wu, Y. (2018). Electrical properties of nanocube CeO$_2$ in advanced solid oxide fuel cells. *International Journal of Hydrogen Energy, 43(28),* 12909–12916. DOI 10.1016/j.ijhydene.2018.05.120.

127. Adijanto, L., Sampath, A., Yu, A. S., Cargnello, M., Fornasiero, P. et al. (2013). Synthesis and stability of Pd@CeO$_2$ core-shell catalyst films in solid oxide fuel cell anodes. *ACS Catalysis, 3(8),* 1801–1809. DOI 10.1021/cs4004112.

128. Tsunekawa, S., Kasuya, A. (2000). Blue shift in ultraviolet absorption spectra of monodisperse CeO_2x nanoparticles. *Journal of Applied Physics, 87(3),* 1318–1321. DOI 10.1063/1.372016.

129. Zhu, X., Yuan, L., Liang, G., Gu, A. (2014). Unique UV-resistant and surface active aramid fibers with simultaneously enhanced mechanical and thermal properties by chemically coating Ce0.8Ca0.2O1.8 having low photocatalytic activity. *Journal of Materials Chemistry A, 2(29),* 11286–11298. DOI 10.1039/c4ta02060j.

130. He, G., Fan, H., Wang, Z. (2014). Enhanced optical properties of heterostructured ZnO/CeO_2 nanocomposite fabricated by one-pot hydrothermal method: fluorescence and ultraviolet absorption and visible light transparency. *Optical Materials, 38,* 145–153. DOI 10.1016/j.optmat.2014.09.037.

131. Liu, F., Wang, C., Su, Q., Zhao, T., Zhao, G. (1997). Optical properties of nanocrystalline ceria. *Applied Optics, 36,* 1796–2798.

132. Zhang, Y. W., Si, R., Liao, C. S., Yan, C. H., Xiao, C. X. et al. (2003). Facile alcohothermal synthesis, size-dependent ultraviolet absorption, and enhanced CO conversion activity of ceria nanocrystals. *Journal of Physical Chemistry B, 107(37),* 10159–10167. DOI 10.1021/jp034981o.

133. Feng, X., Sayle, D., Wang, Z., Paras, M., Santora, B. et al. (2006). Converting ceria polyhedral nanoparticles into single-crystal nanospheres. *Science, 312(5779),* 1504–1508. DOI 10.1126/science.1125767.

134. Joseph, M. S., Shyam, P. M., Ronld, J. G. (1997). *Chemical mechnical planarization of microelectronic materials*. New York: John Wiley & Sons Inc.

135. Hoshino, T., Kurata, Y., Terasaki, Y., Susa, K. (2001). Mechanism of polishing of SiO_2 films by CeO_2 particles. *Journal of Non-Crystalline Solids, 283(1–3),* 129–136. DOI 10.1016/S0022-3093(01)00364-7.

136. Coutinho, C. A., Mudhivarthi, S. R., Kumar, A., Gupta, V. K. (2008). Novel ceria-polymer microcomposites for chemical mechanical polishing. *Applied Surface Science, 255(5),* 3090–3096. DOI 10.1016/j.apsusc.2008.08.093.

137. Deng, H., Hosoya, K., Imanishi, Y., Endo, K., Yamamura, K. (2015). Electro-chemical mechanical polishing of single-crystal *SiC* using CeO_2 slurry. *Electrochemistry Communications, 52,* 5–8. DOI 10.1016/j.elecom.2015.01.002.

138. Finlay, J., Roberts, C. M., Dong, J., Zink, J. I., Tamanoi, F. et al. (2015). Mesoporous silica nanoparticle delivery of chemically modified siRNA against TWIST1 leads to reduced tumor burden. *Nanomedicine-Nanotechnology Biology and Medicine, 11(7),* 1657–1666. DOI 10.1016/j.nano.2015.05.011.

139. Khan, S. B., Faisal, M., Rahman, M. M., Akhtar, K., Asiri, A. M. et al. (2013). Effect of particle size on the photocatalytic activity and sensing properties of CeO_2 nanoparticles. *International Journal of Electrochemical Science, 8,* 7284–7297.

140. Abdel-Hameed, S., Margha, F. H., Ouis, M. (2013). Effect of CeO_2 on the crystallization behavior and magnetic properties of Zn-ferrite glass ceramics. *Journal of Alloys and Compounds, 554,* 371–377. DOI 10.1016/j.jallcom.2012.11.132.

141. Zeng, L. W., Chen, D. Q., Huang, F., Yang, A. P., Lei, L. et al. (2012). Uniform Eu^{3+}: CeO_2 hollow microspheres formation mechanism and optical performance. *Journal of Alloys and Compounds, 534,* 64–69. DOI 10.1016/j.jallcom.2012.04.058.

142. Ji, Z., Shen, X., Zhou, H., Chen, K. (2015). Facile synthesis of reduced graphene oxide/CeO_2 nanocomposites and their application in supercapacitors. *Ceramics International, 41(7),* 8710–8716. DOI 10.1016/j.ceramint.2015.03.089.

143. Das, S., Dowding, J. M., Klump, K. E., McGinnis, J. F., Self, W. et al. (2013). Cerium oxide nanoparticles: applications and prospects in nanomedicine. *Nanomedicine, 8(9),* 1483–1508. DOI 10.2217/nnm.13.133.

144. Mandoli, C., Pagliari, F., Pagliari, S., Forte, G., Di Nardo, P. et al. (2010). Stem cell aligned growth induced by CeO_2 nanoparticles in PLGA scaffolds with improved bioactivity for regenerative medicine. *Advanced Functional Materials, 20(10),* 1617–1624. DOI 10.1002/adfm.200902363.

145. Tarnuzzer, R. W., Colon, J., Patil, S., Seal, S. (2005). Vacancy engineered ceria nanostructures for protection from radiation-induced cellular damage. *Nano Letter, 5(12),* 2573–2577. DOI 10.1021/nl052024f.

146. Chen, J., Patil, S., Seal, S., McGinnis, J. F. (2006). Rare earth nanoparticles prevent retinal degeneration induced by intracellular peroxides. *Nature Nanotechnology, 1(2),* 142–150. DOI 10.1038/nnano.2006.91.

147. Hirst, S. M., Karakoti, A. S., Tyler, R. D., Sriranganathan, N., Seal, S. et al. (2009). Anti-inflammatory properties of cerium oxide nanoparticles. *Small, 5(24),* 2848–2856. DOI 10.1002/smll.200901048.

148. Laosiripojana, N., Chadwick, D., Assabumrungrat, S. (2008). Effect of high surface area CeO_2 and Ce-ZrO_2 supports over Ni catalyst on CH_4 reforming with H_2O in the presence of O_2, H_2, and CO_2. *Chemical Engineering Journal, 138(1–3),* 264–273. DOI 10.1016/j.cej.2007.05.035.

149. Halabi, M. H., de Croon, M. H. J. M., van der Schaaf, J., Cobden, P. D., Schouten, J. C. (2010). Low temperature catalytic methane steam reforming over ceria-zirconia supported rhodium. *Applied Catalysis A, 389(1–2),* 68–79. DOI 10.1016/j.apcata.2010.09.004.

150. Roh, H. S., Eum, I. H., Jeong, D. W. (2012). Low temperature steam reforming of methane over Ni-Ce1-xZrxO$_2$ catalysts under severe conditions. *Renewable Energy, 42,* 212–216. DOI 10.1016/j.renene.2011.08.013.

151. Saqer, S. M., Kondarides, D. I., Verykios, X. E. (2009). Catalytic activity of supported platinum and metal oxide catalysts for toluene oxidation. *Topics in Catalysis, 52(5),* 517–527. DOI 10.1007/s11244-009-9182-8.

152. Kim, K. H., Ihm, S. K. (2011). Heterogeneous catalytic wet air oxidation of refractory organic pollutants in industrial wastewaters: a review. *Journal of Hazardous Materials, 186(1),* 16–34. DOI 10.1016/j.jhazmat.2010.11.011.

153. Amrute, A. P., Mondelli, C., Moser, M., Novell-Leruth, G., López, N. et al. (2012). Performance, structure, and mechanism of CeO_2 in HCl oxidation to Cl_2. *Journal of Catalysis, 286,* 287–297. DOI 10.1016/j.jcat.2011.11.016.

154. Farra, R., Eichelbaum, M., Schlögl, R., Szentmiklósi, L., Schmidt, T. et al. (2013). Do observations on surface coverage-reactivity correlations always describe the true catalytic process? A case study on ceria. *Journal of Catalysis, 297,* 119–127. DOI 10.1016/j.jcat.2012.09.024.

155. Gui, G., Li, J., Zhong, J. (2008). Band structure engineering of graphene by strain: first-principles calculations. *Physical Review B, 78(7),* 75435. DOI 10.1103/PhysRevB.78.075435.

156. Chroneos, A., Yildiz, B., Tarancon, A., Parfitt, D., Kilner, J. A. (2011). Oxygen diffusion in solid oxide fuel cell cathode and electrolyte materials: mechanistic insights from atomistic simulations. *Energy & Environmental Science, 4(8),* 2774–2789. DOI 10.1039/c0ee00717j.